GRANT 142 Vortex Dyn

Final Technical Report

Grant No. NAGW-816 IN-23639

Title of the Grant:

Theoretical and Experimental Investigation of Vortex Breakdown

Principal Investigator:

Prof. Egon Krause, Ph.D.

Period covered by report:

June 1, 1985 - May 31, 1986

Address:

Aerodynamisches Institut
RWTH Aachen
Wüllnerstr. zwischen 5 und 7
5100 Aachen
West Germany

(NASA-CR-176353) THEORETICAL AND EXPERIMENTAL INVESTIGATION OF VORTEX BREAKDOWN Final Technical Report, 1 Jun. 1985 - 31 May 1986 (Technische Hochschule) 47 p CSCL 01A G3/02

N86-31530

Unclas 43281

Introduction

The phenomenon of vortex breakdown is of considerable importance for flows under critical conditions about delta wings. The leading edge vortices on the leeward side of the wing can be termed slender until breakdown is about to occur. The slenderness of the vortices is characterized by the ratio of the core radius R and the length L of the undisturbed vortex, i.e. $R/L \ll 1$. As long as the slenderness condition is satisfied, the equations of motion can be simplified considerably for the description of the flow in the vortex. The integration of the simplified equations is then possible for large Reynolds numbers. The breakdown itself must be analysed by solving the full Navier-Stokes equation. With the slender vortex approximation the overall computation time can be very much reduced, since the largest portion of the flow can be determined from the simplified equations, and extremely fine resolution is only required for the breakdown region, where the full Navier-Stokes equations must be employed.

The work carried out under this contract is concerned with the formulation and solution of the slender-vortex approximation and its numerical solution for incompressible and compressible flow; with the initiation of experimental work and the validation of the solution; and finally the prescription and determination of permissable inflow conditions for the slender-vortex approximation. The results of this analyses are presented in several publications [1] , [2] , [3] , [4] ; copies of the preprints and manuscripts are enclosed.

Formulation of the Problem

The slender-vortex approximation for compressible viscous flow was first formulated in Refs. [1] and [2] . Therein it was shown that the flow is basicly governed by the local axial pressure gradient, which can be expressed through an integro-differential equation. According to this analysis the pressure gradient is mainly determined by the radial distributions of the circumferential velocity component, and the temperature. It could be shown that a hot core tends to stimulate breakdown and that a cold core delays it. The direct influence of the compressibility is that the variable density tries to counteract the influence of positive axial pressure gradients, thereby delaying breakdown.

Permissable Inflow Conditions

The slenderness condition imposed on the flow does not permit one to prescribe arbitrary inflow conditions, which are required for the integration of the simplified equations of motion. The inflow conditions are given by a set of radial profiles for the axial and circumferential velocity profiles, and the temperature. It was shown in [1] and [2] that the inclination of the traces of the stream lines v/u in the axial plane satisfies a second-order nonlinear ordinary differential equation, to be integrated in the radial direction. The coefficients of that equation are solely determined by the inflow conditions. Since the inclination of the traces of the streamlines must obey the slenderness condition, the solution of the equation for v/u decides as to whether or not the prescribed inflow conditions for u, w, and T can be admitted. This is described in detail in Ref. [2].

Numerical Solution

Finite-difference solutions of the slender vortex approximation were developed for incompressible flows, and compressible flows. The differential equations were casted into locally linearized implicit difference equations, which can be inverted by recursion. Details of the solution for incompressible flow are described in [4]; the solution for compressible flow is described in [2], and [3]. The most important results computed with the solution so far are also reported in the references just mentioned: In Ref. [4], it is shown, for example, that the solution reacts sensibly to axial pressure gradients; comparison calculation were carried for the experimental data of Faler and Leibovich. The comparison, discussed in [4] shows that for vorticities with large swirl, the breakdown point cannot be predicted with the slender vortex approoximation, since it does not take into acocunt the upstream influence of the breakdown region.

In Refs. [2] and [3] the results obtained so far for compressible flows are discussed. The influence of the freestream Mach number and of the temperature distribution prescribed for the inflow cross section on the flow development in the downstream direction is clearly demonstrated.

Conclusions

The slender-vortex approximation was analysed for incompressible and com-

pressible flow. First the equations of motion were reduced in an order of magnitude analysis. Then compatiblity conditions were formulated for the inflow conditions. Thereafter finite-difference-solutions were constructed for incompressible and compressible flow. Finally it was shown that these solutions can be used to describe the flow in slender vortices. The analysis of the breakdown process must, however, be excluded, since its upstream influence cannot be predicted with the slender vortex approximation. The investigation of this problem is left for future work.

Literature

[1] E. Krause: "Schlanke Wirbel in kompressibler Strömung". ZAMM, Band 67, Heft 4/5. To be published.

[2] C. H. Liu, E. Krause, S. Menne: "Admissable Upstream Conditions for Slender Compressible Vortices". AIAA / ASME 4th Fluid Mechanics, Plasma Dynamics and Lasers Conference, May 12 - 14, 1986, Atlanta, GA, AIAA-86-1093.

[3] E. Krause, S. Menne, C. H. Liu: "Initiation of Breakdown in Slender Compressible Vortices". 10 International Conference on Numerical Methods in Fluid Dynamics, 23 - 27 June, 1986, Beijing, China. To be published.

[4] L. Reyna, S. Menne: "Numerical Prediction of Flow in Slender Vortices". Accepted for publication in Computers and Fluids.

SCHLANKE WIRBEL IN KOMPRESSIBLER STRÖMUNG

E. Krause

Aerodynamisches Institut der RWTH Aachen
Wüllnerstr. zw. 5 und 7, 5100 Aachen

Der Einfluß der Kompressibilität auf schlanke Wirbel in stationärer, reibungsbehafteter Strömung wird dargestellt. Eine entsprechende Ableitung für reibungsfreie Strömung ist in [1] und für instationäre Strömungen in [2] gegeben.

Für die Untersuchung wird angenommen, daß die Achse des Wirbels parallel zur ankommenden Strömung ist und daß die Strömung im Wirbel rotationssymmetrisch ist. Bezeichnet R den Kernradius in dem Querschnitt senkrecht zur Anströmrichtung, in dem der Wirbel erzeugt wird, und L die unbekannte Länge des Wirbels, gemessen in Strömungsrichtung, über die der Wirbel nicht aufplatzt, so erfordert die Schlankheitsbedingung

$$\frac{v}{u} = O\left(\frac{R}{L}\right) << 1 \qquad (1)$$

Dabei ist v die radiale und u die axiale Geschwindigkeitskomponente. Die mit Gleichung (1) vereinfachten Erhaltungsgleichungen für Masse, Impuls und Energie entsprechen der Grenzschichtapproximation:

Masse:
$$\frac{\partial}{\partial x}(\rho u) + \frac{1}{r}\frac{\partial}{\partial r}(\rho v r) = 0 \qquad (2)$$

Impuls, x-, r- und θ-Richtung:

$$\rho u \frac{\partial u}{\partial x} + \rho v \frac{\partial u}{\partial r} = -\frac{\partial p}{\partial x} + \frac{1}{r}\frac{\partial}{\partial r}\left(r\eta \frac{\partial u}{\partial r}\right) \qquad (3)$$

$$\frac{\rho w^2}{r} = \frac{\partial p}{\partial r} \qquad (4)$$

$$\rho u \frac{\partial \Gamma}{\partial x} + \rho v \frac{\partial \Gamma}{\partial r} = \frac{1}{r}\frac{\partial}{\partial r}\left(\eta r^3 \frac{\partial}{\partial r}\left(\frac{\Gamma}{r^2}\right)\right) \qquad (5)$$

Energie

$$c_p\left(\rho u \frac{\partial T}{\partial x} + \rho v \frac{\partial T}{\partial r}\right) = u\frac{\partial p}{\partial x} + v\frac{\partial p}{\partial r} + \frac{1}{r}\frac{\partial}{\partial r}\left(r\lambda \frac{\partial T}{\partial r}\right) + \eta\left[\left(r\frac{\partial}{\partial r}\left(\frac{\Gamma}{r^2}\right)\right)^2 + \left(\frac{\partial u}{\partial r}\right)^2\right] \qquad (6)$$

Das System wird mit der Zustandsgleichung $\rho = P/(\tilde{R}T)$ geschlossen, wobei $\tilde{R}$ die Gaskonstante ist. Zur Lösung des Gleichungssystems (2)-(6) müssen Einströmbedingungen

$$x = x_0 \;,\; 0 \le r \;:\; u = f_1(r) \quad w = f_2(r) \;,\; T = f_3(r) \qquad (7)$$

Symmetriebedingungen auf der Wirbelachse

$$r = 0 \; ; \; x_0 \leq x \; : \; \frac{\partial u}{\partial r} = v = w = \frac{\partial T}{\partial r} = 0 \; , \tag{8}$$

und Randbedingungen für $r \to \infty$

$$r \to \infty \; , \; x_0 \leq x : \; u = g_1(x) \; , \; w \to 0 \; , \; T \to g_2(x) \tag{9}$$

vorgegeben werden. Die Funktionen $f_1(r) - f_3(r)$ und $g_1(x)$ und $g_2(x)$ müssen als bekannt vorausgesetzt werden.

Wegen der Schlankheitsbedingung (1) können $f_1(r) - f_3(r)$ jedoch nicht willkürlich vorgegeben werden. Dies geht aus folgender Betrachtung hervor: Aus der Kontinuitäts-, Energie- und Zustandsgleichung läßt sich $\frac{\partial u}{\partial x}$ durch folgende Beziehung ausdrücken:

$$\frac{\partial u}{\partial x} = - \frac{u}{\kappa p} \frac{\partial p}{\partial x} - \frac{v}{T} \frac{\partial T}{\partial r} + \frac{(\kappa-1)}{r} \frac{w^2}{a^2} v - \frac{1}{\rho r} \frac{\partial}{\partial r} (\rho v r) + \frac{H}{\rho c_p T} \tag{10}$$

Die Größe H steht zur Abkürzung für die Dissipationsfunktion und den Wärmeleitungsterm in der Energiegleichung. Nach Einsetzen von Gleichung (10) in die x-Impulsgleichung erhält man nach Integration:

$$\frac{v}{u} = \exp(-I) \left[\int_0^r \left[\left(1 - \frac{u^2}{a^2}\right) \frac{1}{\rho u^2} \frac{\partial p}{\partial x} \right] \exp(I) \, dr' \right.$$
$$\left. - \int_0^r \left[\frac{1}{\rho u} \left(\Pi_1 / \rho u - H / c_p T \right) \exp(I) \, dr' \right] \right] \tag{11}$$

Die Größe Π_1 steht zur Abkürzung der Schubspannung in der x-Impulsgleichung und I bedeutet

$$I = \int_0^r \left(1 + \frac{w^2}{a^2}\right) \frac{dr'}{r'} \tag{12}$$

Bei bekannten Einströmbedingungen $f_1(r) - f_3(r)$ kann v/u nach Gleichung (10) bestimmt werden, wenn der örtliche Druckgradient $\partial P / \partial x$ unbekannt ist. Er läßt sich durch Differentation nach x und anschließender Integration aus Gleichung (5) gewinnen:

$$\frac{\partial p}{\partial x}(x,r) = \frac{\partial p}{\partial x}(x, r \to \infty)$$
$$+ \int_r^\infty \left(\frac{\rho w}{r'} \right) \left[\frac{2}{r'} \frac{\partial}{\partial r'} (r' w) - \frac{w}{T} \frac{\partial T}{\partial r'} + \frac{w^3}{c_p T r'} \right] \left(\frac{v}{u} \right) dr'$$
$$- \int_r^\infty \frac{w^2}{a^2 r'} \frac{\partial p}{\partial x} \, dr' - \int_r^\infty \left(2 \Pi_2 - \frac{w}{c_p T} H \right) \frac{w}{r' u} \, dr' \tag{13}$$

Die Größe Π_2 steht zur Abkürzung für die Schubspannung in der θ-Impulsgleichung.

Nach Gleichung (13) ergibt sich stets ein nichtverschwindender Druckgradient $\frac{\partial p}{\partial x}(x,r)$, da in reibungsbehafteter Strömung v/u stets von Null verschieden ist. Ein heißer Kern kann dabei den Druckgradienten vergrößern, während die Umfangskomponente den Druckgradienten verkleinert. Dieser ändert seinen Einfluß mit der axialen Machzahl. Das geht aus der x-Impulsgleichung hervor, die sich in folgende Form bringen läßt:

$$\frac{\partial}{\partial r}\left(\frac{v}{u}\right) = \left(1 - \frac{u^2}{a^2}\right)\frac{1}{\rho u^2}\frac{\partial p}{\partial x} - \left(1 + \frac{w^2}{a^2}\right)\frac{v}{ur} - \frac{1}{\rho u^2}\frac{1}{r}\frac{\partial}{\partial r}\left(r\eta\frac{\partial u}{\partial r}\right) + \frac{(\varkappa-1)}{\rho a^2 u}H \qquad (14)$$

Gleichung (14) zeigt, daß bei Überschalldurchströmung des Wirbels, d.h. u/a > 1 der erste Term sein Vorzeichen ändert.

Sollen nur die Funktionen $f_1(r) - f_3(r)$ auf ihre Kompatibilität mit der Schlankheitsbedingung, Gleichung (1), im Einströmquerschnitt überprüft werden, kann dies durch Elimination der Druckgradienten aus den Impulsgleichungen geschehen: Durch entsprechende Differentation nach x bzw. r und Subtraktion der resultierenden Ausdrücke voneinander, erhält man nach Zusammenfassen

$$\frac{\partial^2}{\partial r^2}\left(\frac{v}{u}\right) + G_1(x,r)\frac{\partial}{\partial r}\left(\frac{v}{u}\right) + G_2(x,r)\left(\frac{v}{u}\right) + G_3(x,r) = 0 \qquad (15)$$

Die Funktionen $G_1(x,r) - G_3(x,r)$ lassen sich unmittelbar aus den Einströmbedingungen ermitteln. Integration von Gleichung (15) ergibt dann die radiale Verteilung v/u, so daß abgeschätzt werden kann, ob die Schlankheitsbedingung, Gleichung (1), erfüllt ist.

Literatur

1. Krause, E., Der Einfluß der Kompressibilität auf schlanke Wirbel, Aerodyn. Institut, RWTH Aachen, Heft 27, S. 19-23, 1985.

2. Krause, E., On Slender Vortices, in: Flow of Real Fluids, G.E.A. Meier, F. Obermeier (Eds.), Lecture Notes in Physics, Vol. 235, Springer Verlag, S. 211-218, 1985.

5.4

PK

NUMERICAL PREDICTION OF FLOW IN SLENDER VORTICES

Luis Reyna* and Stefan Menne**

Aerodynamisches Institut, RWTH Aachen, West Germany

Abstract

We study the slender vortex approximation with attention put on high Reynolds number behaviour. It is shown that the breakdown of the approximation coincides with the criticality condition as introduced by Benjamin [12]. We study free vortices with and without an adverse pressure gradient for viscous and inviscid flows. Finally we compare to experimental results from Faler and Leibovich [8].

* This research was conducted while the first co-author was at the Aerodynamisches Institut as an Alexander von Humboldt-scholar.

** Correspondence and proofs for correction should be transmitted to Stefan Menne, Aerodynamisches Institut, Wüllnerstr. zw. Nr. 5/7, 5100 Aachen, West Germany.

NUMERICAL PREDICTION OF FLOW IN SLENDER VORTICES

Luis Reyna* and Stefan Menne**

Aerodynamisches Institut, RWTH Aachen, West Germany

1. Introduction

Vortex breakdown was initially observed by Peckham and Atkinson [1] for leading edge vortices formed on delta wings at large angle of attack and with large tip angles. The phenomenon has a drastic influence on the aerodynamical behaviour of the flow. In flows around wings its presence strongly decreases the lift [2,3] and in combustion chambers it can be used to design flame holders [4]. Despite of the large amount of research on this subject, the problem of vortex breakdown can not be yet considered as being fully understood. The present state of the art can be found in the review articles by Ludwieg [5], Hall [6] and Leibovich [7].

In experimental investigations Faler and Leibovich [8] found six different cases of breakdown for a swirl flow in a divergent tube. Two of them are nearly axisymmetric and called bubble type, the remaining have either a spiral or helicoidal shape. The spiral form is marked by a kink followed by a cork-screw shaped twisting of the vortex filament. In this case non-axisymmetric effects are important and have to be included in the analysis of the flow [9].

* This research was conducted while the first co-author was at the Aerodynamisches Institut as an Alexander von Humboldt-scholar.

** Correspondence and proofs for correction should be transmitted to Stefan Menne, Aerodynamisches Institut, Wüllnerstr. zw. Nr. 5/7, 5100 Aachen, West Germany.

Vortex breakdown theories assume axial symmetry except Ludwieg's [10] which regards it as a hydrodynamical instability of nearly axisymmetric flow. The important but unanswered question is the dependence of the breakdown type on the approaching flow. In order to explain the phenomenon Squire [11], Benjamin [12,13] and Bossel [14,15] introduced the concept of critical state. The flow is called supercritical when perturbations can only propagate downstream and subcritical when there is an upstream influence. Squire [11] suggested upstream perturbations would accumulate and produce breakdown at the critical state where the flow proceeds from super to subcritical and the phase velocity of the perturbations is zero. Benjamin [12] showed the existence of two equivalent solutions to a conjugate flow, one being supercritical and the other subcritical. He then regards breakdown as a sudden transition from super to subcritical states, similar to the hydraulic jump. It is not possible to predict vortex breakdown with this theory, but it allows a classification of flows. The significance of the theory can be seen in an experimental observation of Faler and Leibovich [8] : "All flows that exhibit vortex breakdown of the "axisymmetric" form (which we classify as types 0 and 1 disturbance forms) or "spiral" form (our type 2) are supercritical upstream, in the sense of Benjamin."

The details of breakdown can be studied by numerical integration of the full Navier-Stokes equations. Lavan, Nielsen and Fejer [16], Kopecky and Torrance [17], Grabowski and Berger [18] computed axisymmetric, laminar, incompressible and stationary swirling flows. Grabowski and Berger [18] found a backward flow for subcritical initial profiles in contrast to the classification of Benjamin [12]. Since the double ring stucture was not present inside the bubble, Faler and Leibovich concluded due to their experiments [19] that the numerical solution should take into account time dependent periodic asymmmetric motions [19]. The time dependent calculation done by Shi [20] showed correctly this structure. The computed flow was stationary upstream of the breakdown point but instationary and nearly time periodic downstream of it. This and similar computations are restricted to low Reynolds numbers, much lower than the ones present in technical applications.

Flow pictures show nearly cylindrical stream surfaces upstream and this observation can be used in order to derive an approximation of the Navier-Stokes equations usually called the slender vortex approximation. The assumption behind this approximation is analogous to the one from boundary layer theory. The slender

vortex approximation has been used by Gartshore [21,22], Hall [23-25], Bossel [26], Mager [27], Nakamura and Uchida [28] and Shi [20]. The approximation based on small gradients and small radial velocities fails at the breakdown point but is valid upstream of it and generally for stable vortices.

The purpose of this paper is to study the high Reynolds number behaviour of the slender vortex approximation. In chapter 2 we prove that the breakdown of the approximation occurs at the critical state as remarked by Ludwieg [5]. In chapter 3 we present numerical solutions for different Reynolds numbers. In the limit of no viscosity the external pressure gradient determines the breakdown. First preliminary results are shown in [29]. Finally we compare to experimental data and discuss the advantages and limitations of the approximation.

2. Slender vortex approximation

Consider now the Navier-Stokes equations written in cylindrical coordinates (x, r, Θ) with corresponding velocities (u,v,w) in a nondimensional form. The axial and radial velocity components are normalized with the axial velocity and the pressure with its value at the initial station for $r \to \infty$. The lengths are normalized with the vortex core radius which marks the region of viscous flow. The circumferential velocity is normalized with its value at the initial station at the edge of the vortex core.

Including the slenderness condition

$$v \ll u \quad , \frac{\partial}{\partial x} \ll \frac{\partial}{\partial r} \tag{1}$$

and assuming steady axial symmetric flow leads to a system of equations

$$u u_x + v u_r + p_x = \frac{1}{Re} \frac{1}{r} (r u_r)_r \tag{2a}$$

$$p_r = \frac{w^2}{r} \tag{2b}$$

$$u w_x + v \frac{1}{r} (rw)_r = \frac{1}{Re} \left[\frac{1}{r}(rw)_r\right]_r \tag{2c}$$

$$(ru)_x + (rv)_r = 0 \tag{2d}$$

called the slender vortex approximation. Here the Reynolds number is based on the vortex core dimension and the undisturbed axial velocity and p is the pressure.

Notice that the type of this system is now parabolic for viscous flow and hyperbolic for inviscid flow coupled to two ordinary differential equations. The first such equation is the momentum equation in the radial direction and the second

$$(rv)_{rr} - \frac{1}{r}(rv)_r + \left[\frac{1}{u^2 r^3}(r^2 w^2)_r - \frac{r}{u}\left(\frac{1}{r}u_r\right)_r\right](rv) = \\ = \frac{1}{Re}\left[-\frac{r}{u}\left(\frac{1}{r}(ru_r)_r\right)_r + \frac{2w}{u^2}\left(\frac{1}{r}(rw)_r\right)_r\right] \tag{3}$$

can be easily derived from (2).

Due to the slenderness condition the approximation based on small gradients and on a small radial velocity fails in the neighbourhood of the breakdown point. According to the theories of Squire [11] and Benjamin [12] the flow is supercritical upstream of this position and perturbations can only propagate downstream. As a consequence the influence of the breakdown bubble is not contained in the slender vortex approximation.

Symmetry conditons are imposed along the r = 0 axis:

$$u_r = 0 \ , \quad v = 0 \ , \quad w = 0 \tag{4a}$$

At the outer radius the type of the system allows three boundary conditions for viscous flow and one for the pressure for inviscid flow; the physical boundary conditions for free vortices are

$$\left(p + \tfrac{1}{2}u^2\right)_{(r,x)} \underset{r\to\infty}{\longrightarrow} C \ , \quad w \underset{r\to\infty}{\longrightarrow} 0 \qquad p \underset{r\to\infty}{\longrightarrow} p_\infty(x) \tag{4b}$$

where C is a constant taken from the initial conditions and $p_\infty(x)$ is the external pressure. These boundary conditions are also valid for the inviscid system when the radial velocity has a negative sign at infinity, otherwise only the pressure can be given

$$p \underset{r\to\infty}{\longrightarrow} p_\infty(x) \tag{4c}$$

The slender vortex approximation in vorticity, circulation, stream-function formulation becomes

$$u\Omega_x + rv\left(\frac{\Omega}{r}\right)_r - \frac{1}{r^3}\Gamma_x^2 = \frac{1}{Re}\left(\frac{1}{r}(r\Omega)_r\right)_r \tag{5a}$$

$$u\Gamma_x + v\Gamma_r = \frac{r}{Re}\left(\frac{1}{r}\Gamma_r\right)_r \tag{5b}$$

$$\Omega = \left(\frac{1}{r}\psi_r\right)_r \tag{5c}$$

with the vorticity $\Omega = -u_r$, local circulation $\Gamma = rw$, stream-function ψ and velocity components

$$u = \varepsilon - \frac{1}{r}\psi_r \tag{6a}$$

$$v = \frac{1}{r}\psi_x \tag{6b}$$

In the vorticity, circulation, stream-function formulation the swirl influence is given explicitly in the vorticity transport equation by the term $^1/_r{}^3\,\Gamma x^2$ in contrast to the formulation in primitive variables where this coupling follows implicitly over the pressure. For an isolated vortex it is advantageous to consider the perturbation of the stream-function from parallel flow. In this case the parameter ε in eq.(6a) is equal to one; else ε is equal to zero.

The boundary conditions (4) corresponding to the vorticity-stream-function formulation are at the axis of symmetry

$$\Omega = 0 \quad , \quad \Gamma = 0 \quad , \quad \psi = 0 \tag{7a}$$

At the outer radius the boundary conditions (4b) translate into

$$\Omega \underset{r\to\infty}{\longrightarrow} 0 \quad , \quad \Gamma \underset{r\to\infty}{\longrightarrow} \beta \quad , \quad \psi_r \underset{r\to\infty}{\longrightarrow} r\left(1-\sqrt{2(C-p_\infty(x))}\right) \tag{7b}$$

where $C = (p_i + \frac{1}{2}u_i^2)$ is a constant taken from the initial conditions and $p_\infty(x)$ is the external pressure. The parameter β specifies the rate of the circumferential velocity at the edge of the vortex core to the axial velocity at infinity in the initial station. These boundary conditions are also valid for the inviscid system when the radial velocity has a negative sign at infinity, otherwise only the pressure can be given

$$p \underset{r\to\infty}{\longrightarrow} p_\infty(x) \tag{7c}$$

Finally for viscous flows in a pipe the no-slip condition

$$u = 0, \quad v = 0, \quad w = 0 \tag{7d}$$

holds at the outer radius.

For free vortices the corresponding boundary conditions for (3) are

$$v = 0 \text{ at } r = 0 \quad \text{and} \quad v_r + \frac{v}{r} + \frac{du_\infty}{dx} = 0 \text{ at } r \longrightarrow \infty \tag{7e}$$

where $u_\infty(x) = \sqrt{2(C-p_\infty(x))}$ is a given function.

Initial conditions have to be provided for the axial and circumferential velocity

$$u(r, x_0) = u_0(r)$$
$$w(r, x_0) = w_0(r) \qquad (7f)$$

The pressure, the radial velocity, the vorticity, the circulation and the stream-function can be obtained from them.

Solutions of the slender vortex approximation can cease to exist due to two different mechanisms: first, when the axial velocity vanishes somewhere in the flow and second, when the radial velocity becomes unbounded. The first case is similar to the boundary layer separation while the second is related to the criticality condition introduced by Benjamin [12]. The second situation arises since there is no viscosity present along the axial direction and therefore unbounded gradients along it can appear. Since the viscosity present in (2) only controls the radial gradients of the axial and circumferential velocity components axial gradients and also the radial velocity can grow infinitely. Moreover, in this case the solution tends to that of the homogeneous problem (3).

$$(rv)_{rr} - \frac{1}{r}(rv)_r + \left[\frac{1}{u^2 r^3}(r^2 w^2)_r - \frac{r}{u}\left(\frac{1}{r}u_r\right)_r\right](rv) = 0 \qquad (8)$$

Indeed numerical solutions of the slender vortex approximation show that the viscous forces are really small compared to pressure and inertia forces near breakdown of the slender vortex equations.

As in boundary layer theory the behaviour of the approximated and the full Navier-Stokes system are identical shortly before breakdown when the proper boundary conditions are imposed. We return to the point when comparing predictions of the slender vortex approximation and experimental results.

We now compare this breakdown condition to the criticality condition as introduced by Benjamin [12] (see also Hall [6]).

Benjamin considers steady, inviscid and axisymmetric flow. Introducing the streamfunction ψ with $u = \frac{1}{r}\psi_r$ and $v = -\frac{1}{r}\psi_x$, the total head $h = p + \frac{1}{2}(u^2+v^2+w^2)$ and the circulation $\Gamma = rw$ the equation of motion for these flows can be summarized in a single equation for the stream-function.

$$\frac{\partial^2\psi}{\partial x^2} + \frac{\partial^2\psi}{\partial r^2} - \frac{1}{r}\frac{\partial\psi}{\partial r} = -\Gamma\frac{d\Gamma}{d\psi} + r^2\frac{dh}{d\psi} \qquad (9)$$

We now consider a perturbation of a quasicylindrical flow

$$\Psi_{(x,r)} = \Psi_{(x,r)} + \varepsilon F_{(x,r)} e^{\gamma x} \qquad (10)$$

where $\varepsilon \ll 1$ and $\frac{\partial F}{\partial x} \ll \frac{\partial F}{\partial r}$. This perturbation introduced in (9) and neglecting higher order terms in ε yields an equation for F. The critical state F_c corresponds to $\gamma = 0$ and in this case

$$F_{c_{rr}} - \frac{1}{r} F_{c_r} + \left[-\frac{r}{\mu} \left(\frac{1}{r} \mu_r \right)_r + \frac{1}{r^3 \mu^2} (r^2 w^2)_r \right] F_c = 0 \qquad (11)$$

If the solution with initial data $F_c = 0$ and $F_{cr} = 1$ at r=0 vanishes away from the axis the flow is subcritical; when this solution vanishes at both the axis and outer radius R it is said to be critical and otherwise supercritical.

In comparison to eq.(11) the equation for the radial velocity (8)

$$(rv)_{rr} - \frac{1}{r}(rv)_r + \left[-\frac{r}{\mu} \left(\frac{1}{r} \mu_r \right)_r + \frac{1}{r^3 \mu^2} (r^2 w^2)_r \right] (rv) = 0 \qquad (12)$$

shows an identical form with the boundary conditons

$$v = 0 \text{ at } r = 0 \text{ and } v_r + \frac{v}{r} + \frac{d\mu_\infty}{dx} = 0 \text{ at } r = R \qquad (13)$$

where the outer radius R has a finite value with $R \gg 1$.

The general solution of eq.(12) reads

$$(rv) = C\, H(r) \qquad (14)$$

where the boundary condition $(rv)_{(r=0)} = 0$ is already used.

With the constant C the solution function $H_{(r)}$ can be adapted to the boundary condition at r=R. Excluding the trivial solution $v \equiv 0$, i.e. $v_{(r=R)} \neq 0$, the demand

$$r \longrightarrow R : \quad H \longrightarrow 0$$

leads to a critical case, since necessarily the constant C has to go to infinity and consequently

$$0 < r < R : \quad (rv) \longrightarrow \infty$$

This characteristical behaviour of the radial velocity is present in the slender vortex approximation in the vicinity of the breakdown region. A comparison of this critical case with the previously described critical flow state according to the theory of Benjamin [12] leads to a complete agreement: eq.(11) and (12) are equivalent to each other just as the boundary and the criticality conditions since the condition $F_{cr} = 1$ excludes only the trivial solution.

Now we can see that the breakdown condition for the slender vortex approximation corresponds to the condition from Benjamin [12] and breakdown can be seen as a transition from supercritical to subcritical flows as remarked by Ludwieg [5]. Hall [6] reached also the same conclusion. He explained the equivalence using the existence of two solutions for the slender vortex a small distance apart from each other which do not coincide as the distance tends to zero. He then shows that "the condition for the appearence of arbitrarily large axial gradients turn out to be identical to the condition for the critical" [6].

3. Solution and results

We used both the primitive variables and the vorticity-stream function formulation for the numerical solution of the slender vortex approximation. In a first approach we used primitive variables with centered discretization. The radial velocity is evaluated only at the midpoints of axial intervals (see fig. 1). The discretization only use two "time" levels making it convenient for variable axial spacing. The function value distribution is shown in fig. 1.

Here f_{ij} denotes the numerical solution at the (i,j) node corresponding to $(x,r) = (i\Delta x, j\Delta r)$, where Δx and Δr are the axial and radial spacing. The equations are solved marching along the axial direction as the type of the system indicates it. At each new axial station a system of nonlinear equations must be solved. This is done using Newton's approach and a linear band solver for the Jacobian inversion.

In order to decrease the band width, the symmetry condition for the axial velocity is applied as

$$u_r = \frac{u_{i+1,1} - u_{i+1,0}}{\Delta r} + \frac{\Delta r}{4} Re\left[\frac{u^2_{i+1,0} - u^2_{i,0}}{2\Delta x} + \frac{P_{i+1,0} - P_{i,0}}{\Delta x}\right] + O(\Delta r^2) \quad (15)$$

instead of three point extrapolation formula. (This boundary condition also holds in the inviscid case). The discretization is second order accurate in both radial and axial direction and unconditionally stable with respect to the size of Δx.

Nevertheless during the calculation the size of Δx is decreased when the Courant-Friedrichs-Lewy number $CFL = \max_i \frac{v_i}{u_i} \frac{\Delta x}{\Delta r}$ exceeds a predetermined constant CFL_{max}. Δx is also decreased when the Newton's procedure fails to reduce the residual below the tolerance limit TOL after NEW_{max} iterations.

Normally we use $CFL_{max}=2$, $NEW_{max}=3$ and $TOL=10^{-4}$, being the solution not sensitive to these values.

The second numerical approach was applied to the vorticity stream-function formulation (6). We use again centered discretization with function values determined at node points except the radial velocity which is evaluated at intermediate axial points $(i+\frac{1}{2},j)$ (Crank-Nicolson formulation). The resulting discretization is unconditionally stable and second order accurate. At each new axial station a tridiagonal system must be solved for the stream-function, vorticity and circulation. For a free vortex the equations are not coupled through the boundary conditions and therefore can be solved iteratively as follows. We initialize

$$\begin{aligned} u^{(0)}_{i+1,j} &= u_{i,j} \\ v^{(0)}_{i+1/2,j} &= v_{i-1/2,j} \end{aligned} \qquad (16)$$

and using these values compute $\Gamma^{(1)}$ and then $\Omega^{(1)}$.

Next the stream-function $\psi^{(1)}$ is computed and a new iteration can be started. The procedure is repeated until

$$\max_j \left\{ u^{(n+1)}_{i+1,j} - u^{(n)}_{i+1,j} \right\} \leq \varepsilon \quad , \quad \varepsilon \ll 1 \qquad (17)$$

where ε is usually set to $10^{-4} \sim 10^{-5}$. The iterative procedure has a low storage requirement, only two axial stations has to be kept. It has the drawback to be only convergent for supercritical profiles. This is not the case for the Newton's-iteration approach that allows subcritical initial profiles. On the other hand initially subcritical profiles are of little physical interest since these flows can be regarded as already broken down according to the theories of Squire [11] and Benjamin [12].

The convergence problem translates into increasing number of iterations as the flow reaches criticality conditions. In these situations the axial step is decreased in order to keep the amount of work low; this also gives a better axial location for the breakdown point. Each line the axial step is decreased, the iteration is restarted with the last converged values.

Since few grid points are required outside the vortex core we use a transformation in the radial direction

$$r : (0, r_{max}) \longrightarrow \sigma : (0, \sigma_{max})$$

$$\frac{r}{r_{max}} = \frac{\tan\left(\frac{\pi}{2}\sigma\right)}{\tan\left(\frac{\pi}{2}\sigma_{max}\right)} \tag{18}$$

The uniform spacing in the σ -direction gives almost a uniform distribution in the radial direction when $\sigma_{max} \ll 1$ and an accumulation of grid points near the axis when $\sigma_{max} \approx 1$. The pressure is obtained integrating the radial momentum equation

$$P_{i,j} = P_{i,j+1} - \left[-\frac{1}{24}(g_{j-1} + g_{j+2}) + \frac{13}{24}(g_j + g_{j+1})\right] \tag{19}$$

where

$$g_j = \frac{\Gamma_{i,j}^2}{r_j^2 \tilde{P}_j} \quad \text{and} \quad \tilde{P}_j = \frac{2}{\pi r_{max}} \tan\left(\frac{\pi}{2}\sigma_{max}\right) \cos^2\left(\frac{\pi}{2}\sigma\right)$$

The initial value is the pressure at σ_{max}. g is an even function of σ. In order to decrease the truncation error the pressure is integrated analytically outside the vorticity core where the circulation is constant.

The initial values are taken as

$$u_0 = 1 + \alpha f(r) \quad \text{with} \quad f(r) = \begin{cases} 1 - 6r^2 + 8r^3 - r^4 & , r \le 1 \\ 0 & , r > 1 \end{cases} \tag{20}$$

$$w_0 = \beta g(r) \quad \text{with} \quad g(r) = \begin{cases} r(2 - r^2) & , r \le 1 \\ \frac{1}{r} & , r > 1 \end{cases}$$

These polynomial distributions are already used by Mager [27], Grabowski and Berger [18] and Shi [20] and "...were chosen to approximate the experimentally-measured velocity in vortex cores such as those of trailing vortices..." [18].

The parameter α controls the shape of the axial profile, uniform flow for $\alpha = 0$, jetlike for $\alpha > 0$ and wakelike for $\alpha < 0$. The circulation corresponds to solid body rotation for $r \ll 1$ and to potential flow outside the core of vorticity. The polynomials fulfill symmetry conditions and provide a smooth transition form the

solidly rotating core into the outer flowfield. The parameter β specifies the rate of the circumferential velocity at the edge of the vortex core to the axial velocity at infinty in the initial station.

We now return to the boundary conditions for free vortices. We assume constant pressure gradient

$$\frac{dp_\infty}{dx} = \tau \tag{21}$$

Then the slender vortex equations can be scaled using

$$\tilde{x} = x \cdot \tau \quad , \quad \tilde{v} = \frac{v}{\tau} \quad , \quad \tilde{Re} = Re \cdot \tau \tag{22}$$

and therefore the pressure gradient for the transformed system is equal to one. The flow is relevant for values $\tilde{x} < \frac{1}{2}$ since the outer continuitly desacceleration of the outer flow makes the outer axial velocity vanish at $\tilde{x} = \frac{1}{2}$.

When no pressure gradient is present in the outer flow the scaling

$$\tilde{\tilde{x}} = \frac{x}{Re} \quad , \quad \tilde{\tilde{v}} = v\,Re \tag{23}$$

makes the equations and the initial conditions Reynolds number independent. Notice that the axial coordinate is stretched but the radial coordinate is left unchanged in contrast to boundary layer type of scaling (e.g. Hall [25]). The result is an increasing breakdown length for increasing Reynolds number in contrast to experimental observations [30] for which the location reaches a limit. Due to this behaviour at high Reynolds number we do not expect this to be the physical mechanism behind breakdown which we believe to be pressure induced.

For tube flows the numerical procedure for the stream-function formulation was slightly changed due to coupling of the vorticity and stream-function through boundary conditions. The stream-function was computed from the fourth order differential equation obtained when (6c) is introduced in (6a) and using a five point centered discretization. For the primitive variable formulation these new boundary conditions introduced no new complications.

In order to resolve the boundary layer on the tube wall, the following stretching function was used

$$r = R_{(x)} \frac{2}{\pi \sigma_m} \arctan\left(\sigma \tan\left(\frac{\pi}{2}\sigma_m\right)\right) \tag{24}$$

with $R_{(x)}$ being the tube radius and $\sigma_m = 0.8$.

Faler and Leibovich [8] measured several velocity distributions which were used as initial condition for the flow calculations.

We study our breakdown criterion described in chapter 2 by applying it to free flows driven by a pressure gradient which reach critical state already in the initial section. We used simplified profiles that allow us to do analytical work:

$$u_0 = \begin{cases} 1+\alpha, & r \le \frac{1}{2}\sqrt{2} \\ 1, & r > \frac{1}{2}\sqrt{2} \end{cases}, \quad w_0 = \begin{cases} 2\beta r, & r \le \frac{1}{2}\sqrt{2} \\ \frac{\beta}{r}, & r > \frac{1}{2}\sqrt{2} \end{cases} \tag{25}$$

These profiles are an approximation to the profiles used in the numerical examples. The axial velocity distribution is discontinous and the circumferential velocity can be described by solid body rotation inside the core and potential flow outside of it.

Introducing these distributions in (12) we obtain

$$\begin{aligned} &Z^2 v_{zz} + Z v_z + (Z^2-1) v = 0 && \text{for } r \le \tfrac{1}{2}\sqrt{2} \\ \text{and} \\ &\left(\tfrac{1}{r}(rv)_r\right)_r = 0 && \text{for } r > \tfrac{1}{2}\sqrt{2} \end{aligned} \tag{26}$$

where

$$Z = \frac{4\beta}{1+\alpha} r$$

Since the axial velocity is discontinous jump conditions have to be prescribed [31]:

$$\left[\frac{v}{u}\right]^* = 0 \quad \text{and} \quad \left[\frac{u^2}{r}\left(\frac{rv}{u}\right)_r\right]^* = 0 \quad \text{at} \quad r_0 = \tfrac{1}{2}\sqrt{2} \tag{27}$$

where $[f]^*$ denotes the jump in the values of f across r.

The solution of eq.(16) reads

$$\begin{aligned} v &= c_1 J_1(Z) && \text{for } r \le \tfrac{1}{2}\sqrt{2} \\ v &= c_2 r + \frac{c_3}{r} && \text{for } r > \tfrac{1}{2}\sqrt{2} \end{aligned} \tag{28}$$

where J_1 is the Bessel function of the first kind of first order. The constant c_2 is determined by the pressure gradient at infinity. Since the condition $v = 0$ at $r = 0$ is already used, the constants c_1 and c_3 are determined by the jump conditions (27).

It follows

$$c_1 J_1\left(\frac{4\beta r}{1+\alpha}\right) = (1+\alpha)\left(c_2 r + \frac{c_3}{r}\right) \quad \text{from } \left[\frac{v}{u}\right]^* = 0 \tag{29a}$$

$$C_1 = \frac{2\,C_2}{4\beta\, J_0\left(\frac{4\beta r_c}{1+\alpha}\right)} \qquad \text{from } \left[\frac{u^2}{r}\left(\frac{rv}{u}\right)_r\right]^* = 0 \qquad (29b)$$

at $r_0 = \frac{1}{2}\sqrt{2}$

Criticality is already reached when

$$J_0\left(\frac{4\beta}{1+\alpha}\,\frac{1}{2}\sqrt{2}\right) = 0 \qquad (30)$$

that is

$$\alpha_G = \frac{2\sqrt{2}}{j_{0,0}}\beta - 1 \qquad \text{with } j_{0,0} \approx 2.405 \qquad (31)$$

($j_{0,0}$ is the first non trivial zero of the zeroth Bessel function J_0). This critical curve is drawn in figure 2 as a dotted line. The curve marked by triangles shows the numerical profiles which are initially critical. Due to the undershoot in the axial velocity for $\alpha < 0$ of the discontinuous analytical distribution when compared to the numerically used profiles, the limiting curve lies too high producing a destabilizing effect ($\alpha > 0$ produces the inverse effect). The overshoot of the analytically used profiles for the circulation shifts the curve $\alpha_G(\beta)$ upwards. The numerical results can be summarized as follows: Or the right side of the limiting curve in fig. 2 no solution of the slender vortex approximation can be found (subcritical region). At the left there exists a region where vortices have a limited breakdown length. In the following region at the left no vortex breakdown appears at all. The vortices are stable and dissipate themselves away.

3.1. Isolated vortex for inviscid and viscous flow

Figs. 3-6 show results for the free vortex with $\alpha = 0$, $\beta = .8$ and $\left(\frac{dp}{dx}\right)_{r=\infty} = 0$. This vortex breaks down at $\frac{x}{Re} = 0.013$. In fig. 3 we show the relative strength of the forces present in the axial momentum balance. Here F_p is the pressure force, F_I the inertia and F_V the viscous force. Initially pressure and inertia forces are almost equal while viscous forces are much smaller. Near breakdown both pressure and inertia forces show a dramatic increase in their strength. This increase is not

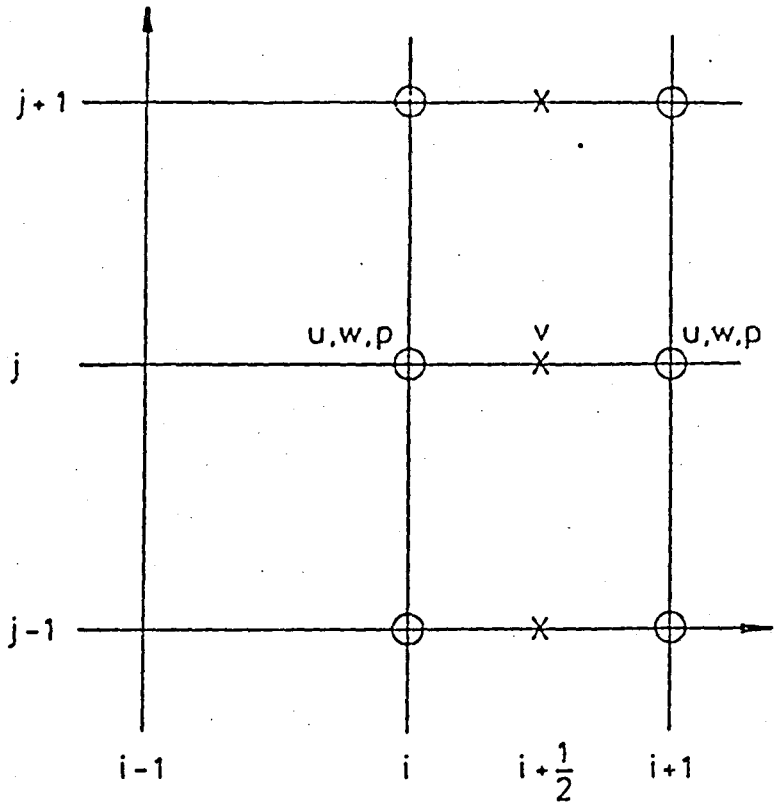
j+1
j
j-1
u,w,p
v
u,w,p
i-1
i
i+1/2
i+1

Fig. 1.

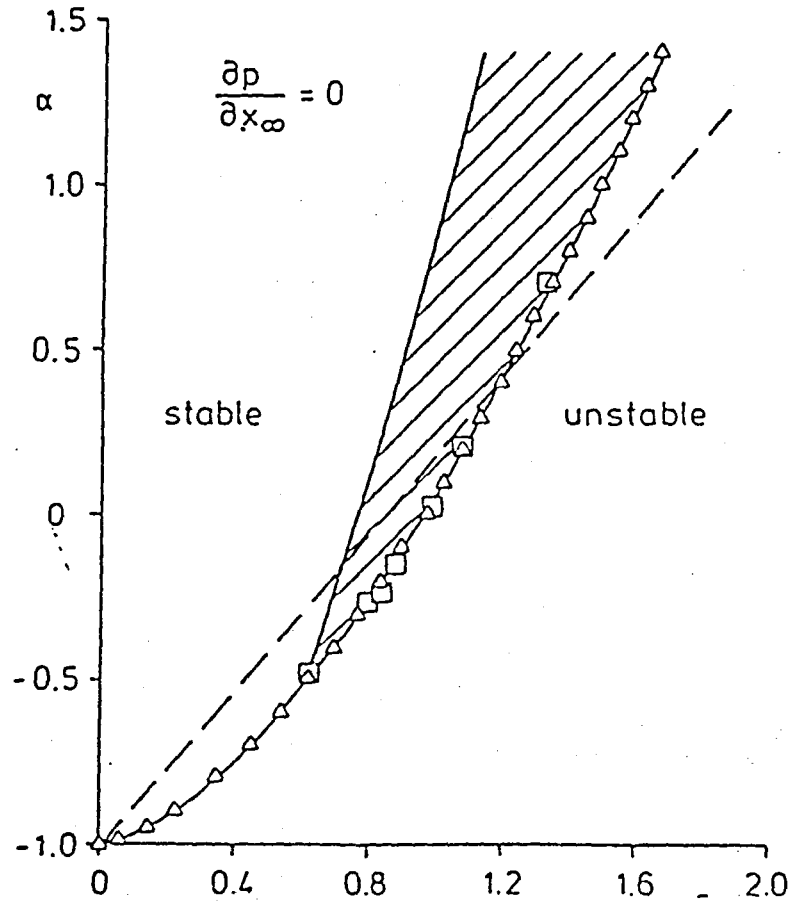
1.5
α
1.0
0.5
0
-0.5
-1.0
∂p/∂x∞ = 0
stable
unstable
0
0.4
0.8
1.2
1.6
2.0

Fig. 2.

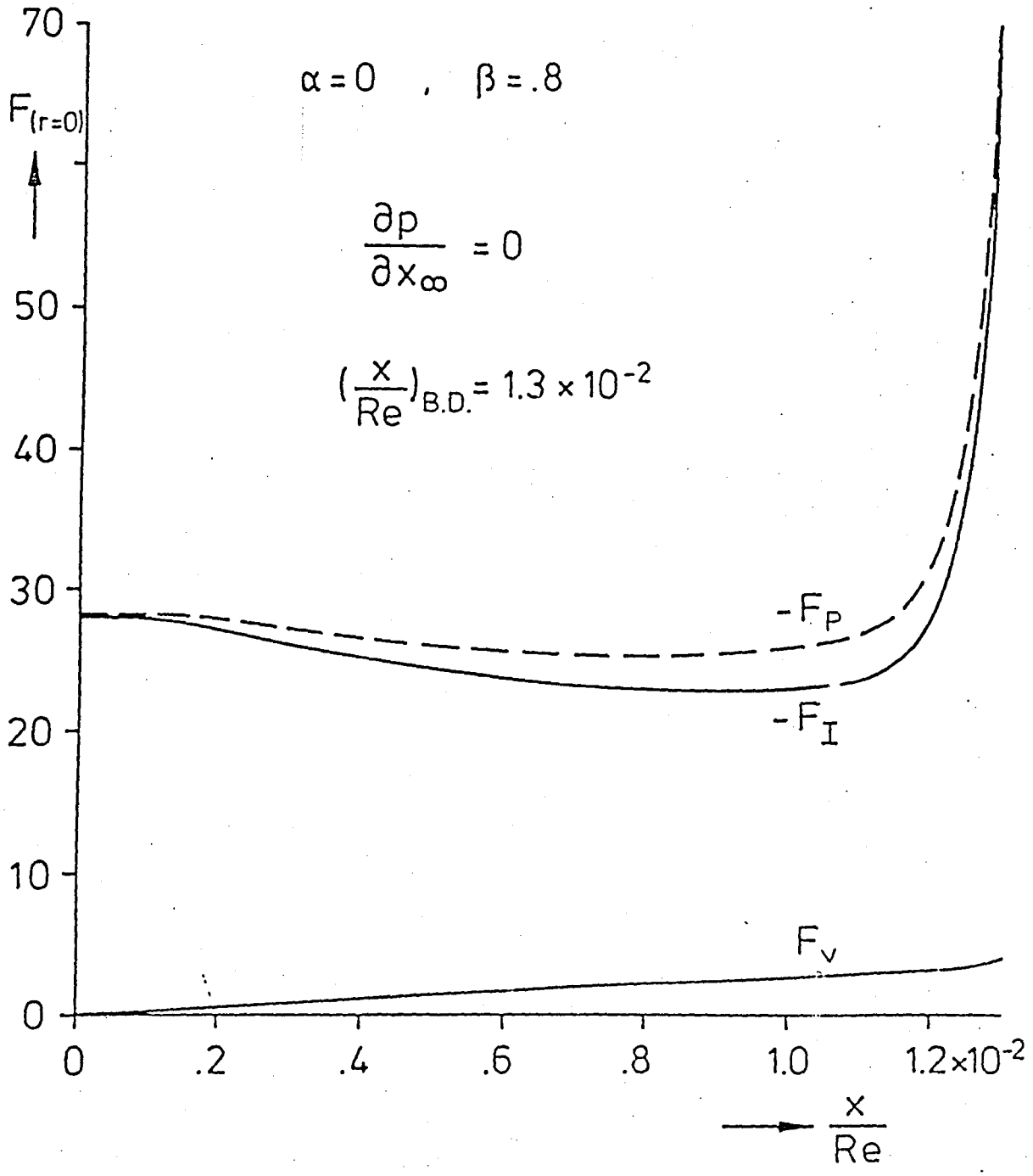
70
$F_{(r=0)}$
50
40
30
20
10
0
$\alpha = 0$, $\beta = .8$
$\frac{\partial p}{\partial x_\infty} = 0$
$(\frac{x}{Re})_{B.D.} = 1.3 \times 10^{-2}$
$-F_P$
$-F_I$
F_v
0
.2
.4
.6
.8
1.0
1.2×10^{-2}
$\frac{x}{Re}$

Fig. 3.

present in the viscous forces. Near breakdown the flow is essentially inviscid, viscosity plays a secondary role. This is in agreement with the corresponding theories of Squire [11] and Benjamin [12] and the critical condition which calls for a non trivial solution to the homogeneous version of equation (3).

Fig. 4 shows the radial dependence of the three components of the velocity vector at different axial stations. The circumferential velocity decreases in magnitude and the axial velocity develops a wakelike profile as the flow reaches breakdown conditions. The radial velocity shows a dramatic increase just before breakdown, similar to that of the pressure and inertia forces. Fig. 5 presents the radial distribution of the pressure. The behaviour of the pressure is quite similar to that of the axial and circumferential velocity component. Fig. 6 shows the axial distribution of the pressure and of the radial velocity at different radial distances from the symmetry axis. Notice an almost linear change in the pressure until shortly before breakdown. In fig. 7 and 8 the velocity components and the pressure are shown at different axial stations for inviscid flow. Fig. 9 demonstrates the axial dependence of the pressure for inviscid flow. The good agreement of the breakdown process compared to the viscous case indicates that breakdown is an inviscid phenomenon.

Fig. 10 shows the dependence of the breakdown length on the initial profiles for free vortices without adverse pressure gradient. Here only supercritical profiles are considered. We also show the corresponding results obtained by Shi [20] by solving the time dependent Navier-Stokes equations. The slender vortex approximation is in good agreement with his numerical results.

For a given β, there exists a lower bound for α leading to initially supercritical profiles. It is possible nevertheless to numerically solve system (2) starting with subcritical profiles when using primitive variables in conjunction with a direct solver. We found that all such flows exhibit breakdown at some axial distance from the initial profile.

The increase of the jet type profile provides a stabilizing effect on the flow. For α large enough and passed a critical value the vortex does not break down at all and viscosity only flattens the profiles (this is usually referred as aging of the vortex) (see fig. 11). The effects of α on the flow are still important near its critical value. For α passed this value the axial velocity at the axis decreases initially but after reaching a minimum value increases again with no breakdown of the flow.

There is no unbounded growth in either the pressure gradient or the radial velocity any longer.

$$\alpha = 0 \quad , \quad \beta = .8 \quad , \quad \frac{\partial p}{\partial x_\infty} = 0 \quad , \quad \left(\frac{x}{Re}\right)_{B.D.} = 1.3 \times 10^{-2}$$

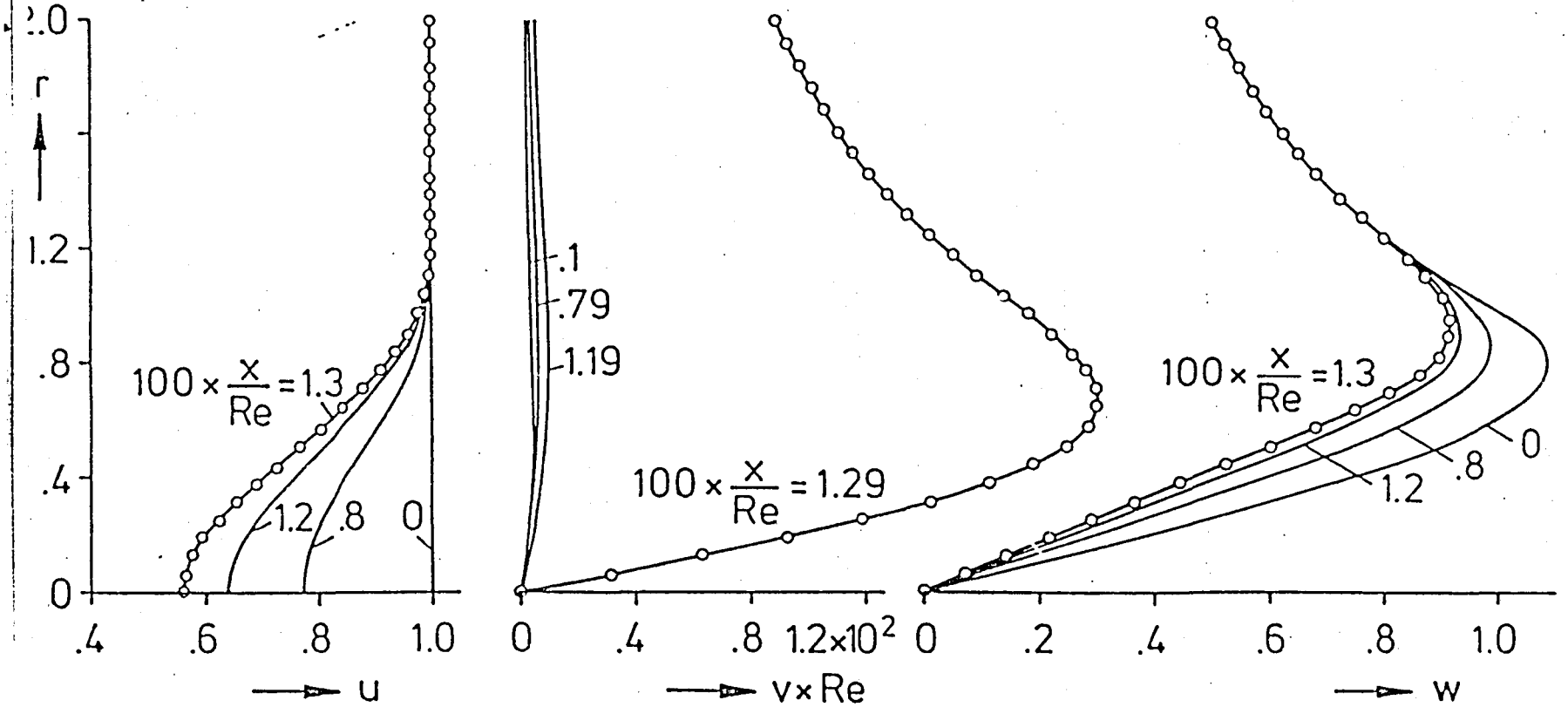

Fig. 4.

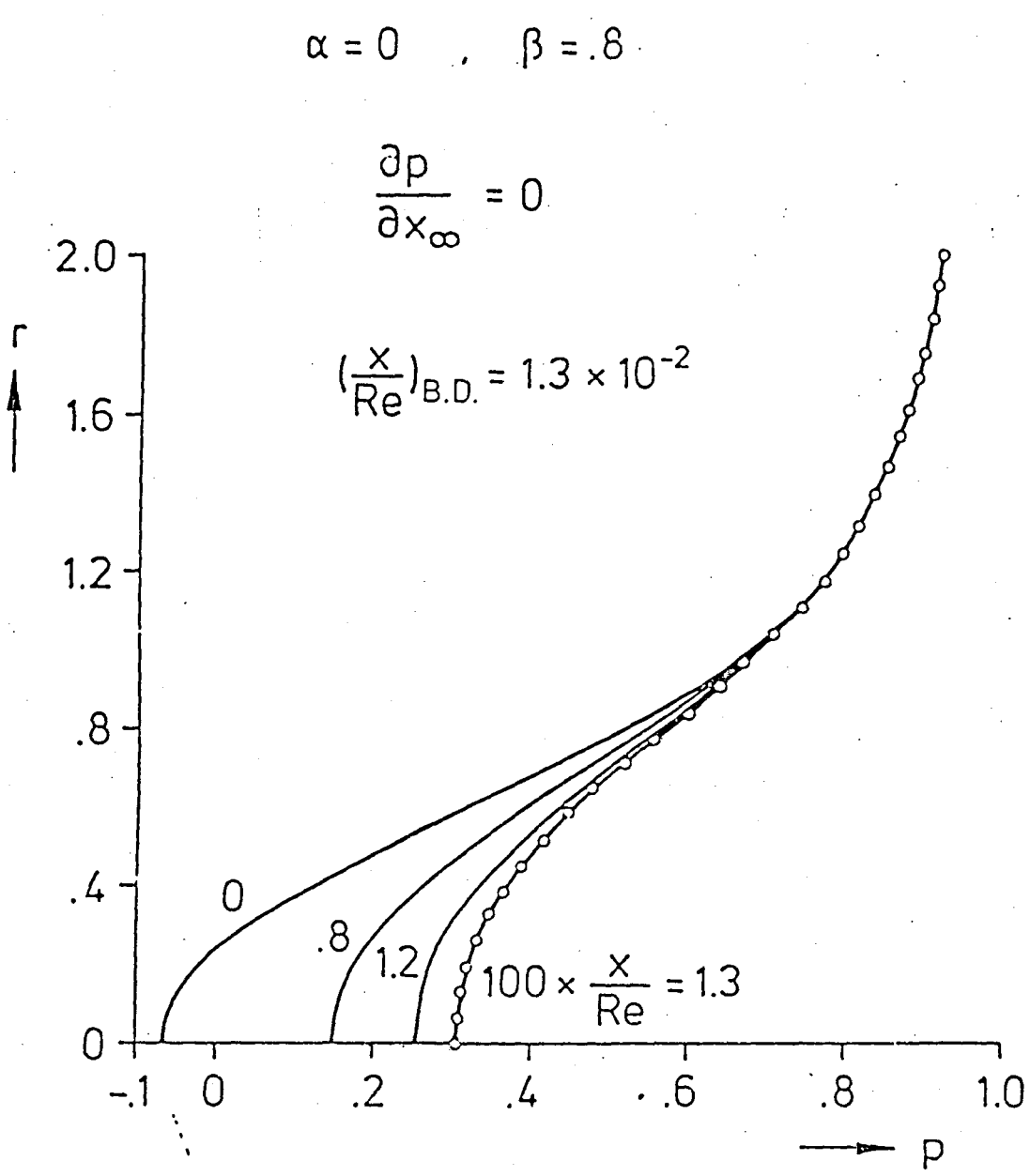

Fig. 5.

$\alpha = 0$, $\beta = .8$, $\frac{\partial p}{\partial x_\infty} = 0$, $\left(\frac{x}{Re}\right)_{B.D.} = 1.3 \times 10^{-2}$

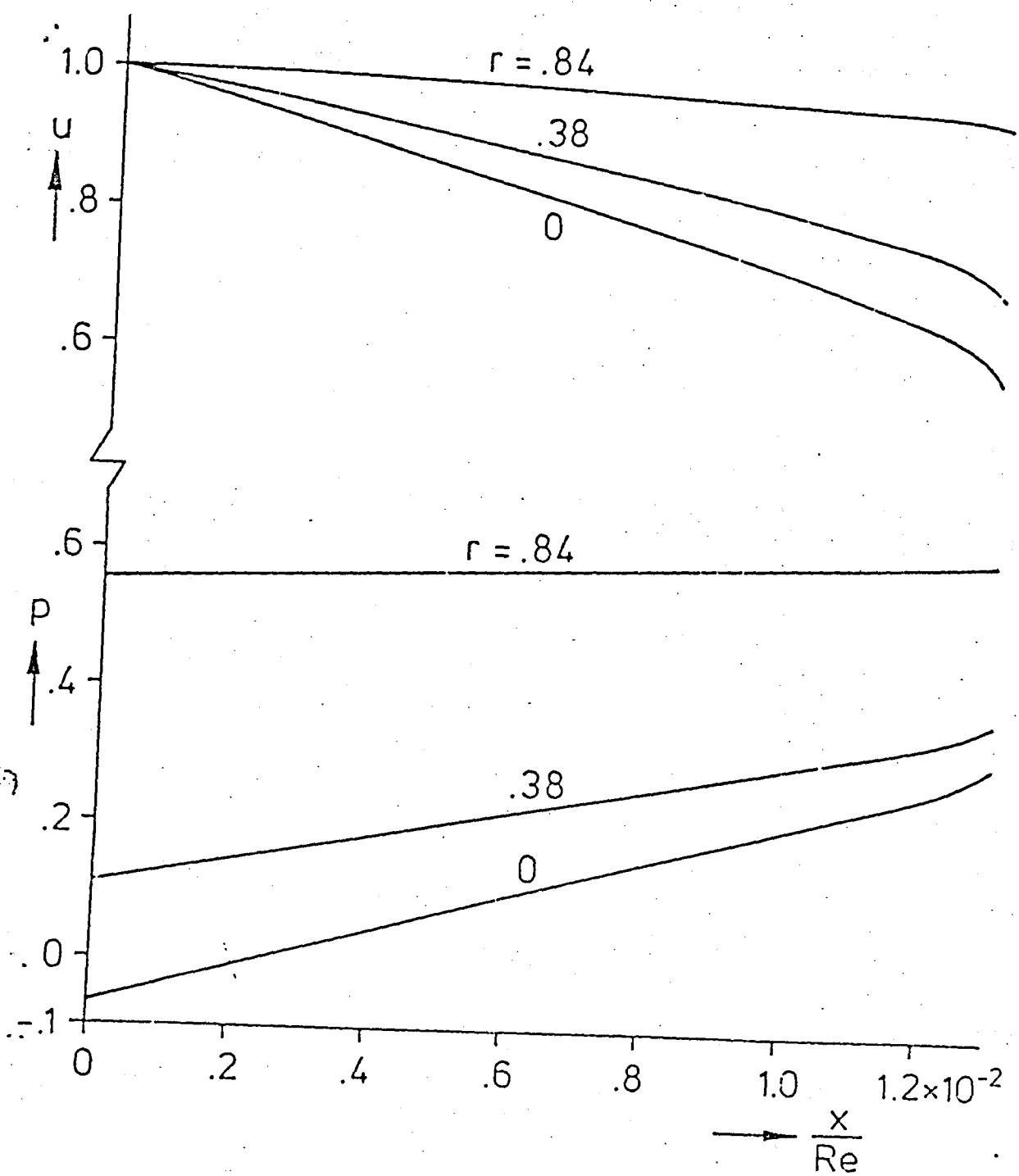

Fig. 6.

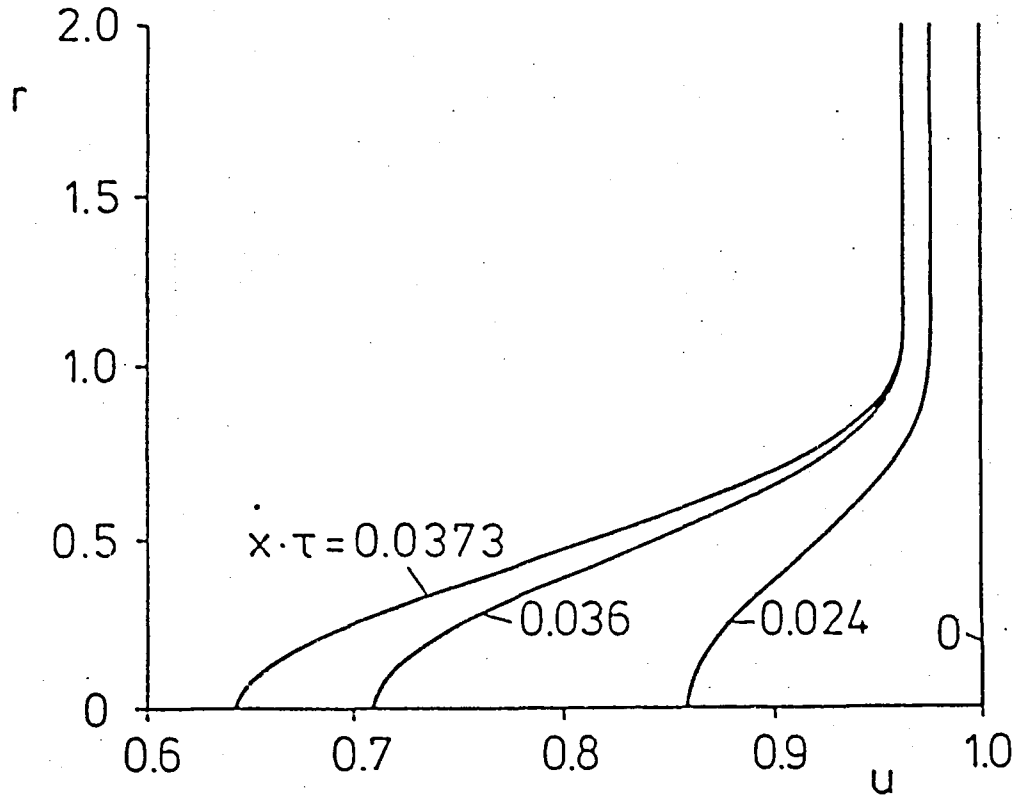
2.0
r
1.5
1.0
0.5
0
x·τ = 0.0373
0.036
0.024
0
0.6
0.7
0.8
0.9
1.0
u

Fig. 7(a).

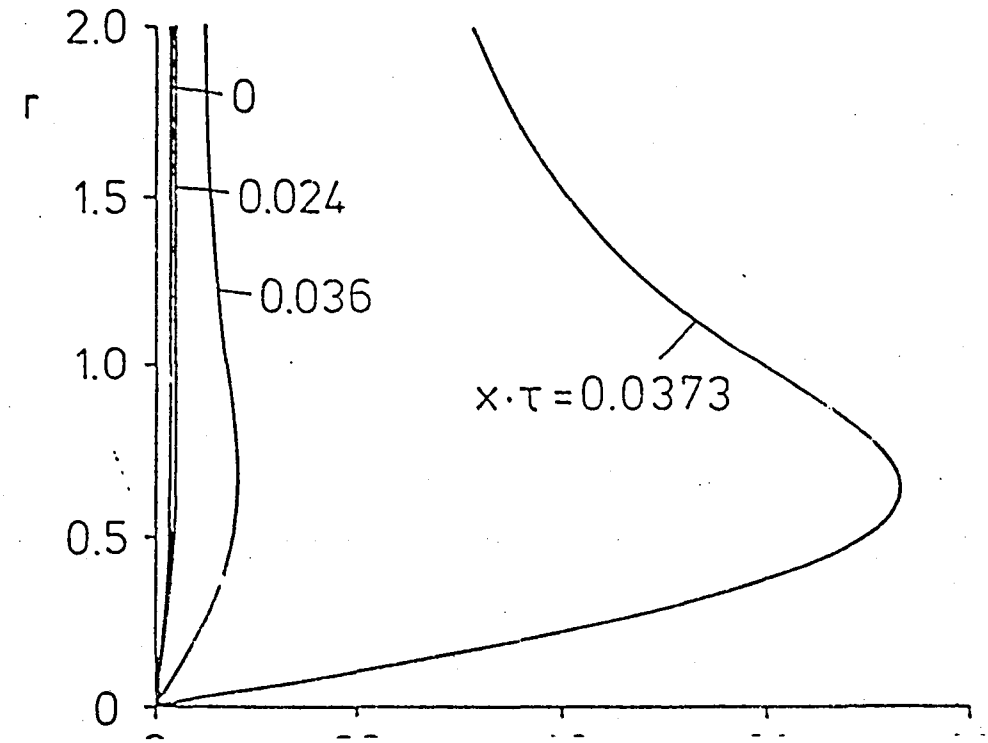
2.0
r
1.5
1.0
0.5
0
0
0.024
0.036
x·τ = 0.0373

Fig. 7(b).

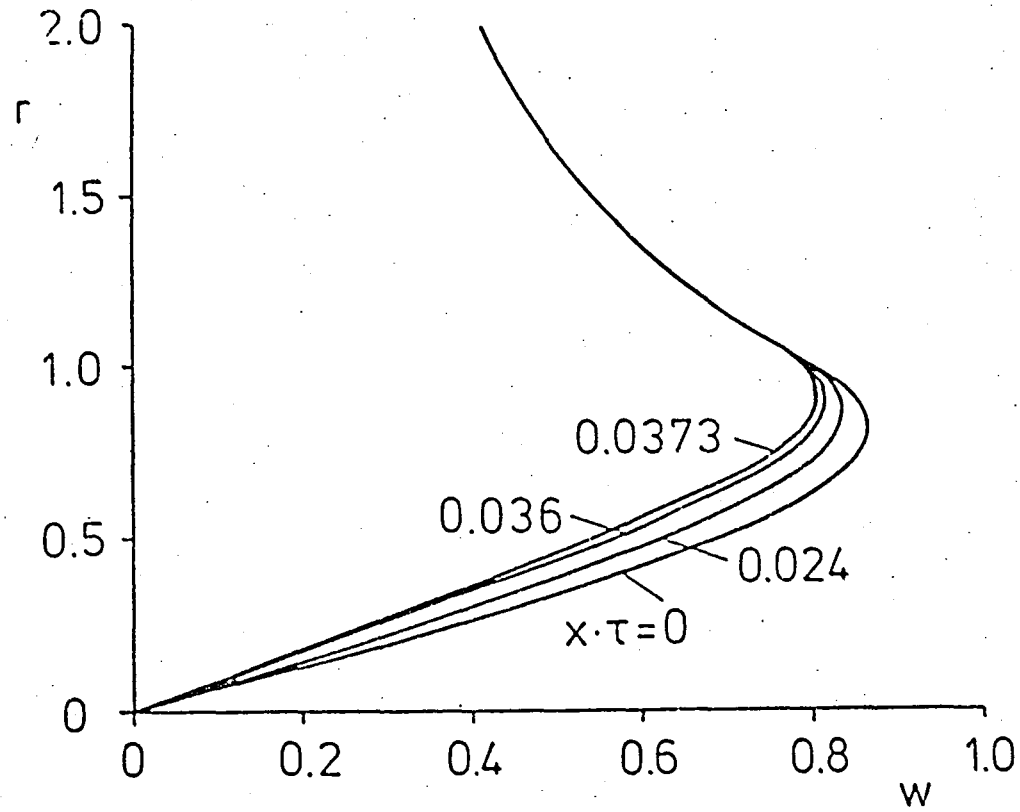
2.0
r
1.5
1.0
0.5
0
0.0373
0.036
0.024
x·τ=0
0
0.2
0.4
0.6
0.8
1.0
w

Fig. 7(c).

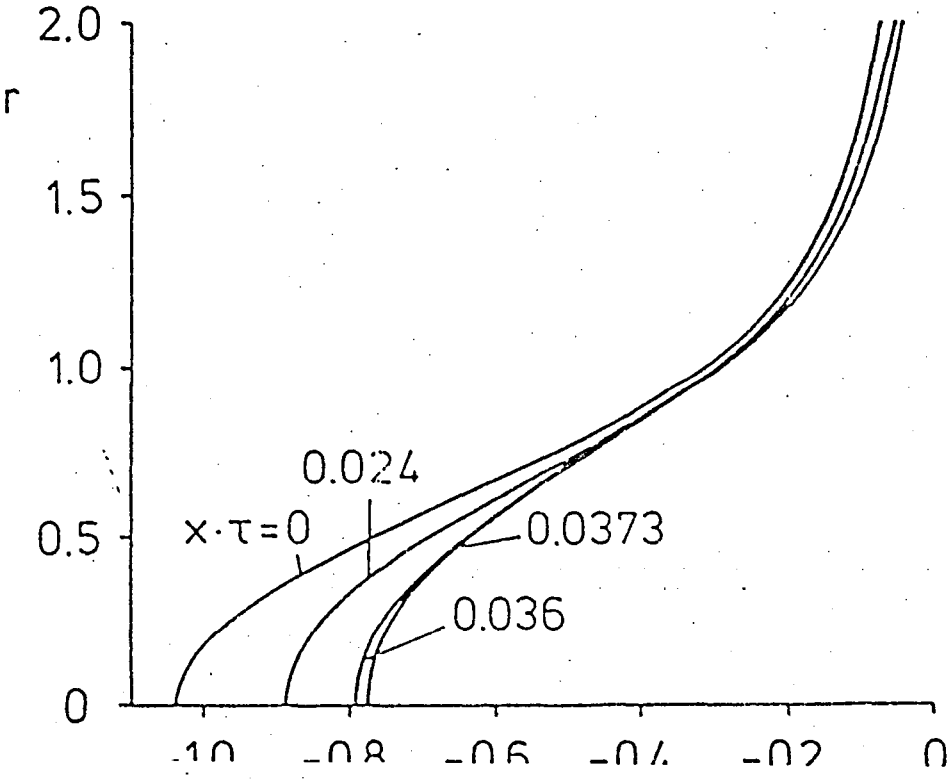
2.0
r
1.5
1.0
0.5
0
0.024
x·τ=0
0.0373
0.036
-1.0
-0.8
-0.6
-0.4
-0.2
0

Fig. 8.

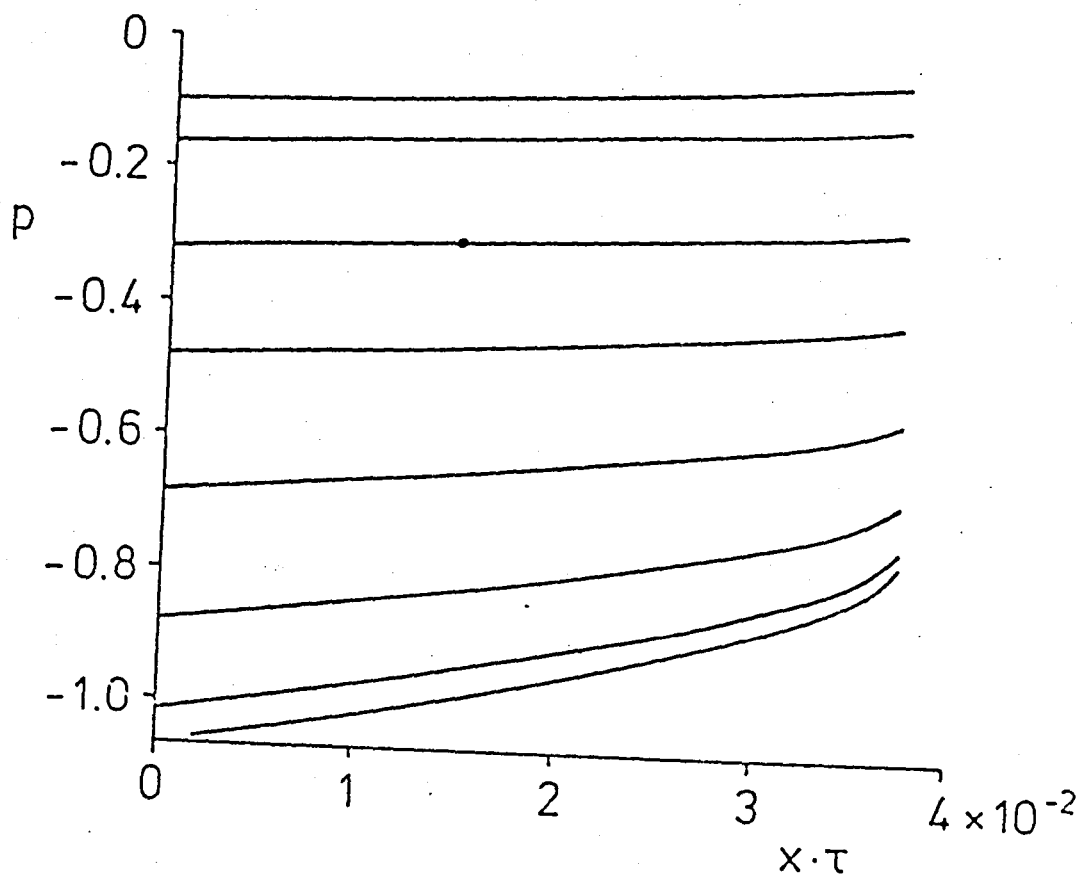

Fig. 9.

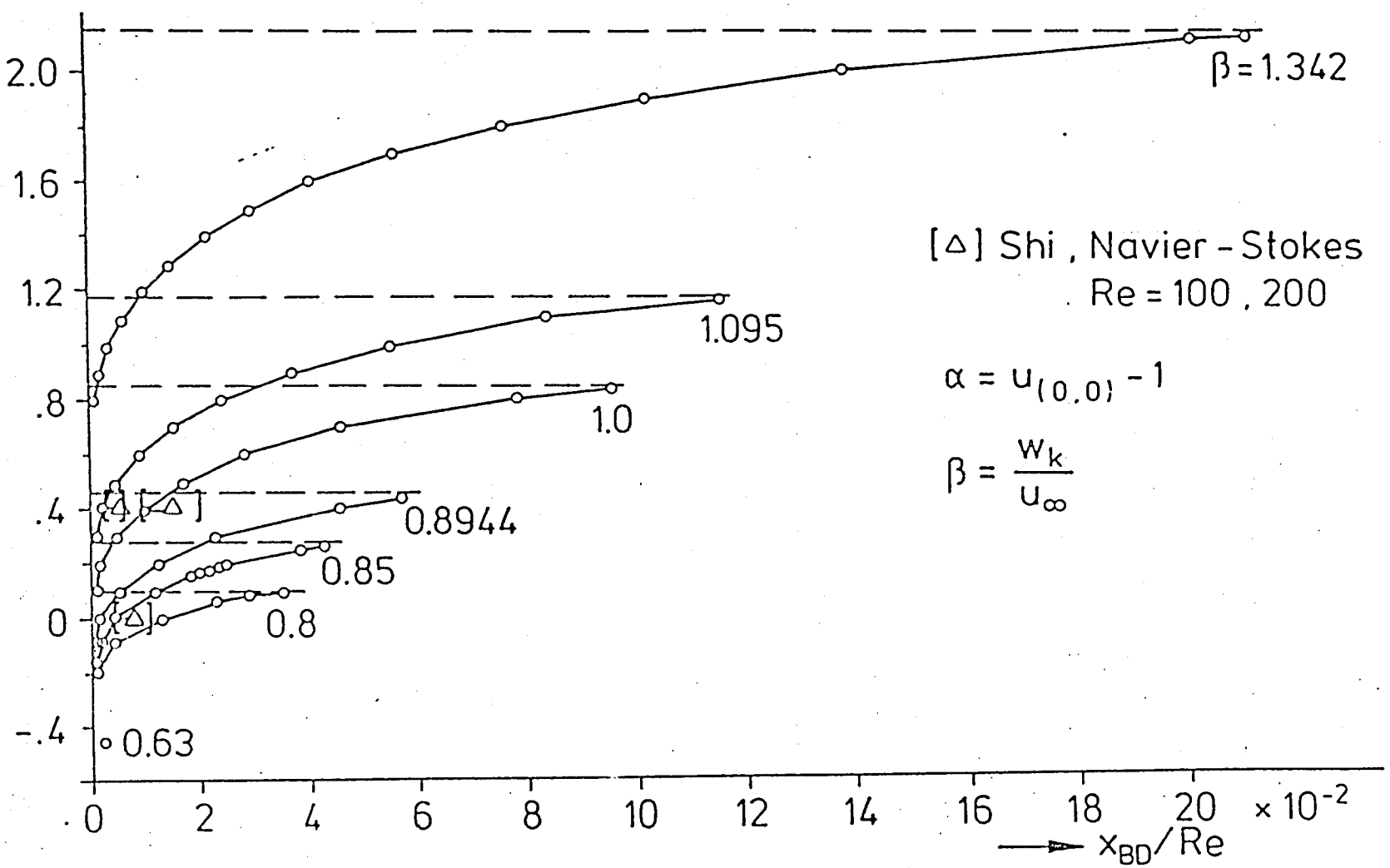
2.0
1.6
1.2
.8
.4
0
-.4
β = 1.342
1.095
1.0
0.8944
0.85
0.8
0.63
[Δ] [Δ]
[Δ] Shi , Navier - Stokes
Re = 100 , 200
α = u(0,0) - 1
β = wk / u∞
0 2 4 6 8 10 12 14 16 18 20 × 10-2
xBD / Re

Fig. 10.

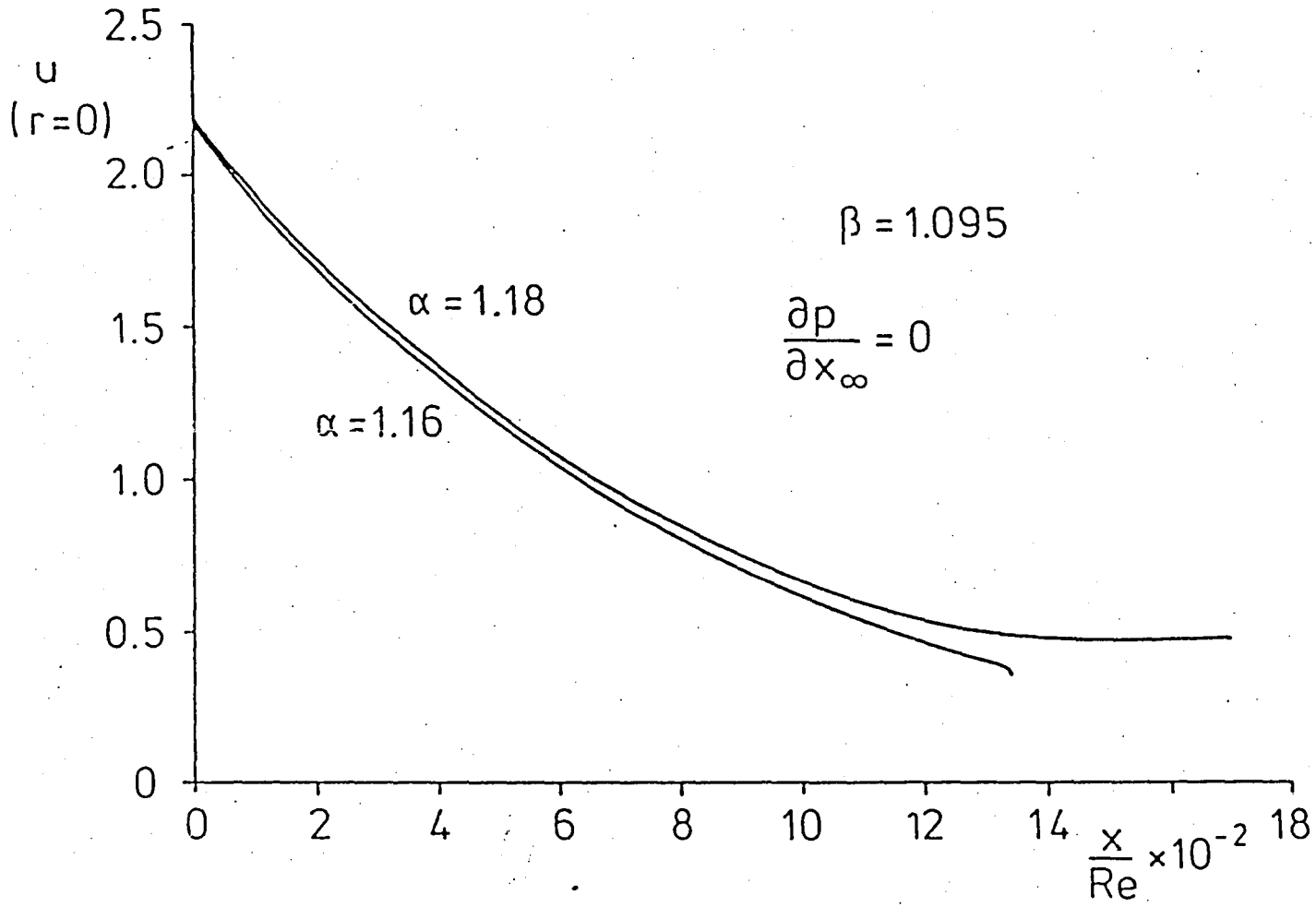
2.5
u
(r=0)
2.0
1.5
1.0
0.5
0
0
2
4
6
8
10
12
14
18
$\frac{x}{Re} \times 10^{-2}$
$\beta = 1.095$
$\frac{\partial p}{\partial x_\infty} = 0$
$\alpha = 1.18$
$\alpha = 1.16$

Fig. 11.

Fig. 12 shows results for vortices with constant external pressure gradient $\frac{dp}{dx}_{r=\infty} = \tau$ and fig. 12a an increase in the breakdown length for increasing Reynolds number with its value attaining a limit for $Re \to \infty$. This is the expected behaviour for vortices that exhibit breakdown without external pressure gradient. Vortices that are stable in absence of pressure gradient (here $\alpha = 1.1$) can break down for $Re \cdot \tau$ large enough (in this case $Re \cdot \tau \gtrsim 0.1$) but are stable otherwise, as once more expected.

Fig. 12b shows the dependence of the breakdown length for small pressure gradient. For τ small we can see x_{BD}/Re reading the expected values obtained from the vortex without pressure gradient shown in fig. 10. For increasing Reynolds numbers the ratio x_{BD}/Re tends to zero since x_{BD} tends to the limit shown in the left picture. Fig. 13a and 13b show similar results obtained from different swirls. We can see again the disappearence of breakdown for stable vortices for small enough pressure gradients.

In order to stress the influence of the pressure gradient on the flow we sketch in fig. 14 the results from figs. 10, 12 and 13 combined for $Re \cdot \tau = 10$. The flow is shown to be extremely sensitive to small pressure fluctuations at large Reynolds numbers. A change in 1% in the pressure, normalized with the dynamic head, over one vortex core length translates into a 100% change in the breakdown length for a Reynolds number of 1000.

The behaviour of the flow shown in figs. 12 and 13 can also be found in experimental investigations. Werlé [29] found that the breakdown length of a leading edge vortex formed on a delta wing does not change for high Reynolds numbers ($Re_L > 10^4$) for an angle of attack of 20 degrees. If we assume that the adverse pressure gradient of the vortex lies approximately in the range of 0.5 to 2% of the dynamic head over the vortex core radius, then the value of $Re \cdot \tau$ lies between 50 and 200.

For these values the breakdown length has approximately reached its ultimate value accepted for $Re \cdot \tau \to \infty$ (Fig. 12a and 12b). The extreme sensitivity against adverse pressure gradients shown in fig. 14 can be observed also in fig. 15 (from [30]). Although the obstacle is positioned far downstream of the breakdown point, there is a significant change in the breakdown length.

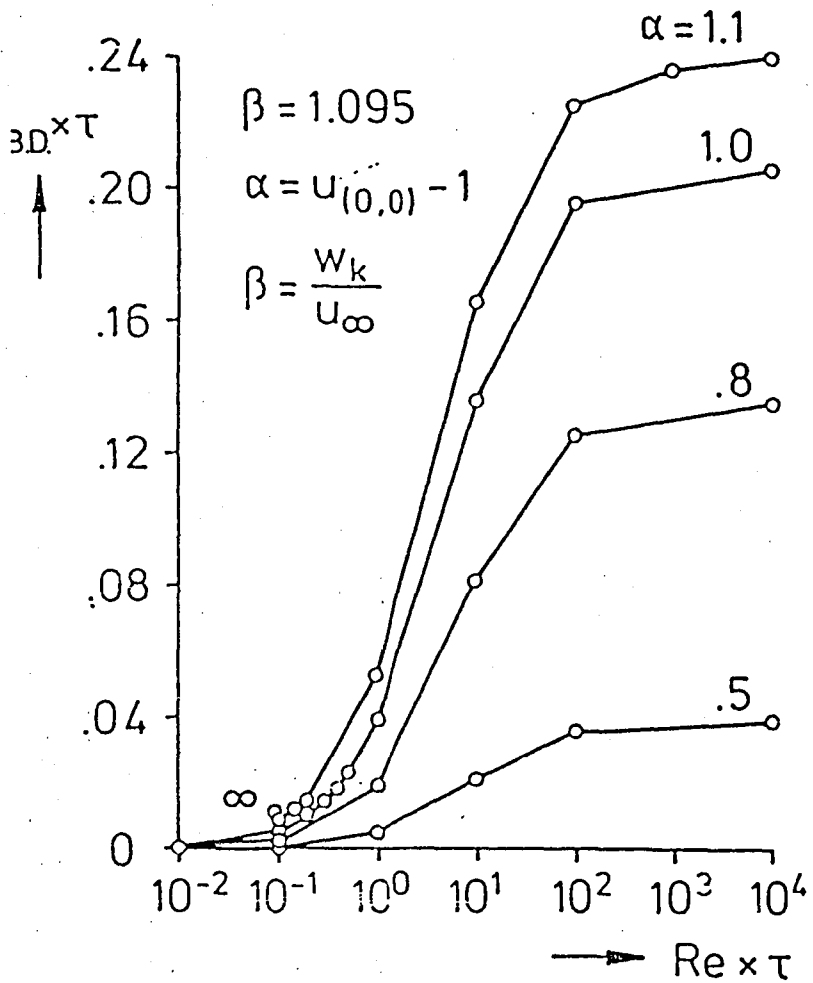

Fig. 12(a).

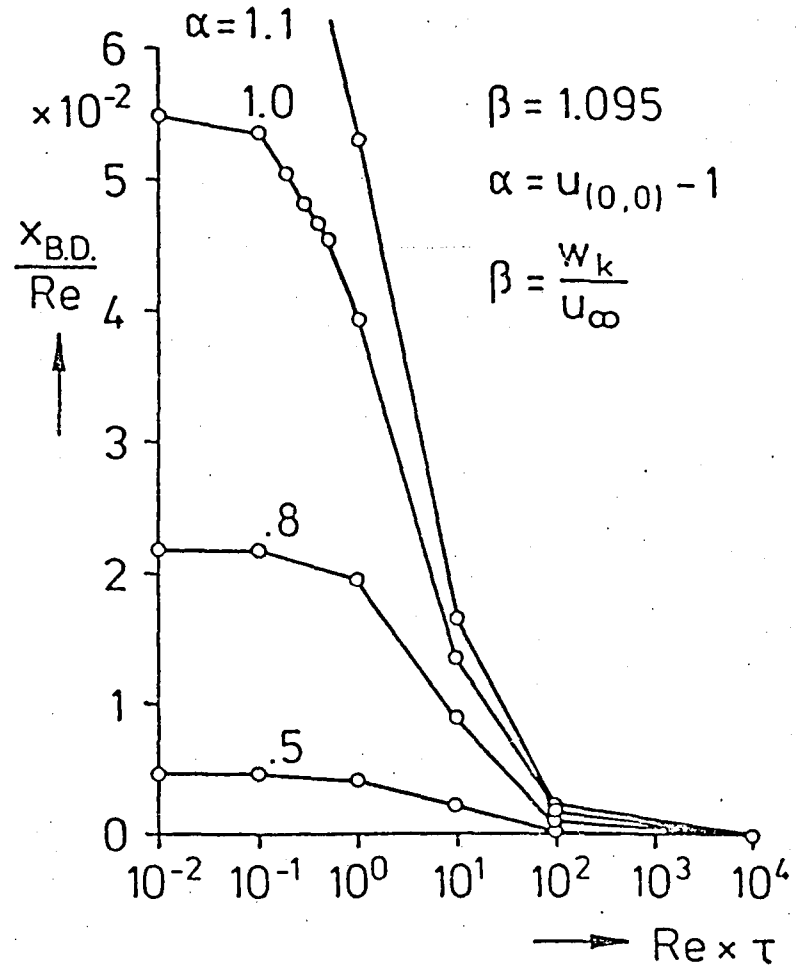

Fig. 12(b).

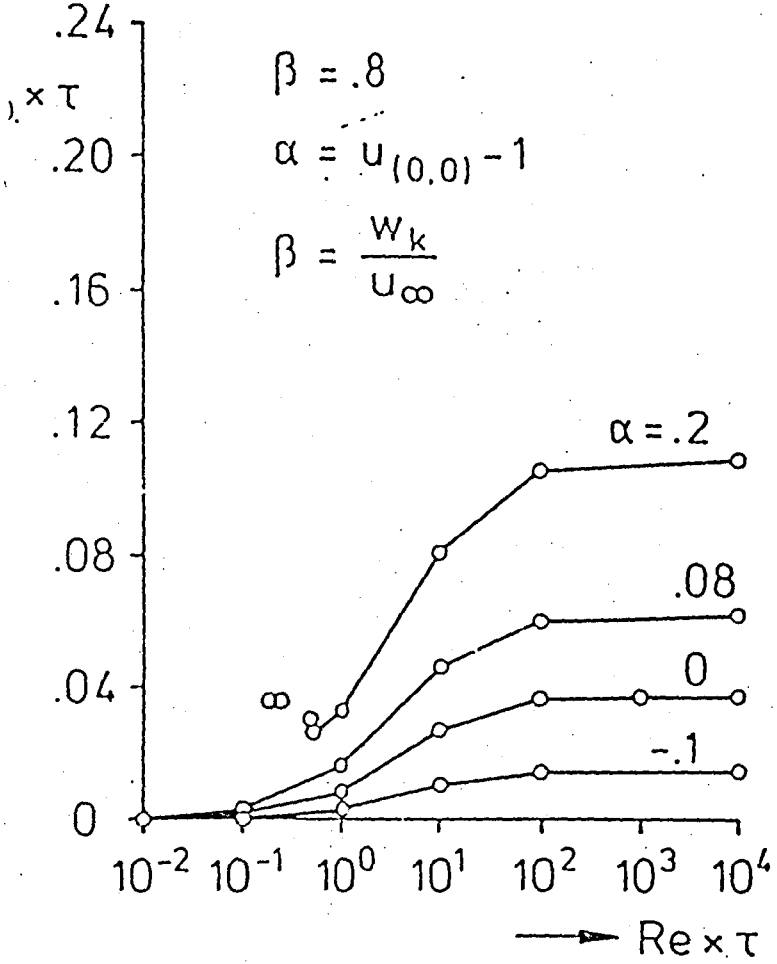

Fig. 13(a).

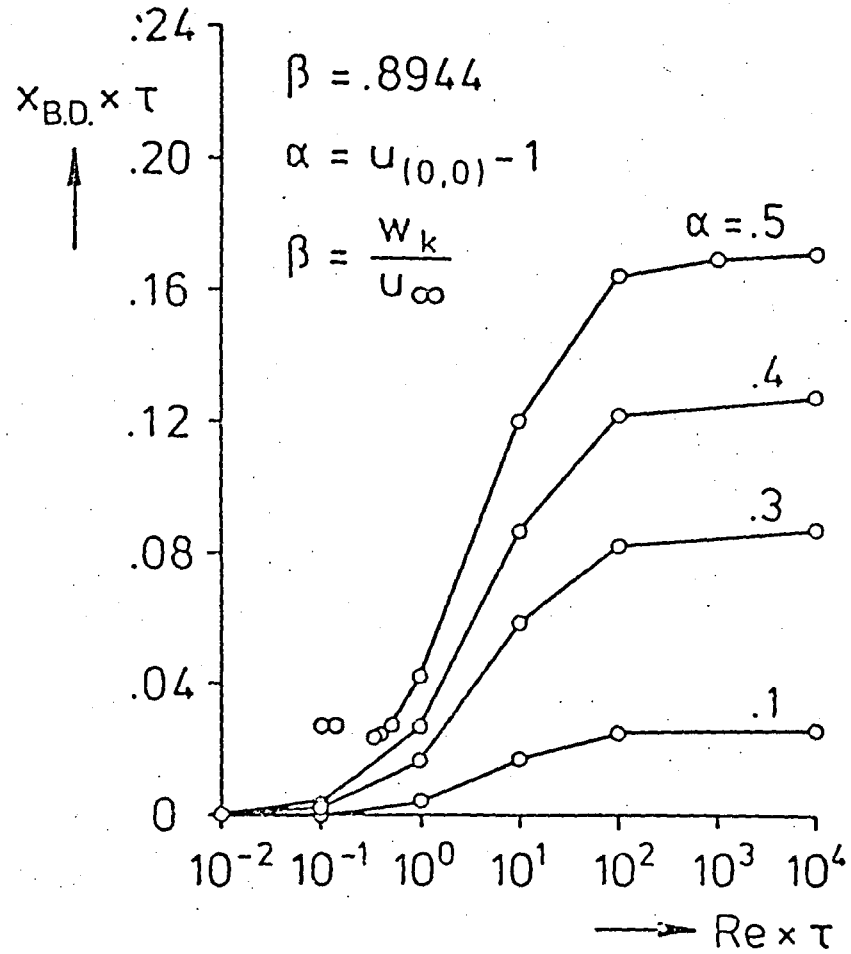

Fig. 13 (b).

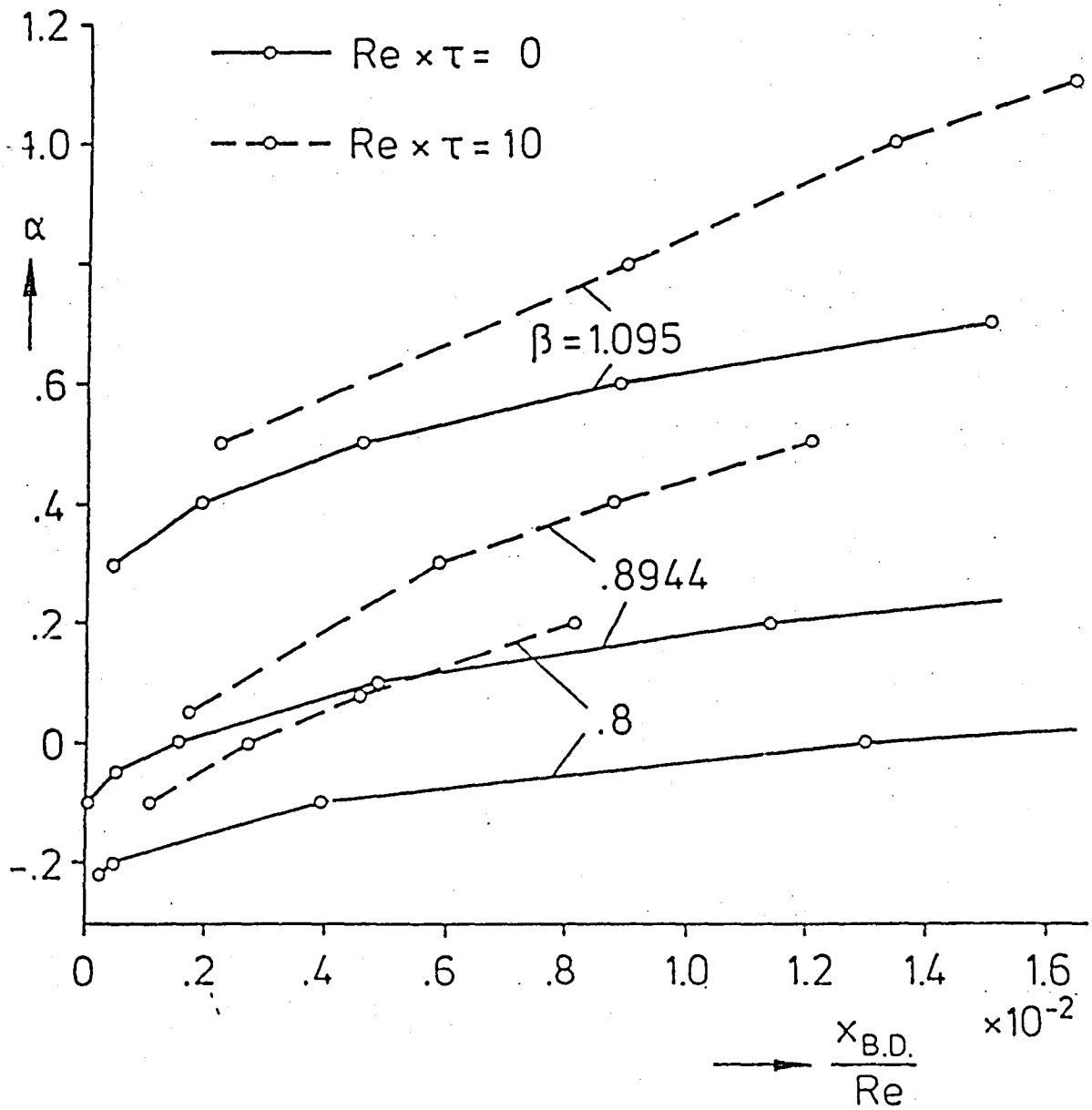
Re × τ = 0
Re × τ = 10
β = 1.095
.8944
.8
α
1.2
1.0
.6
.4
.2
0
-.2
0
.2
.4
.6
.8
1.0
1.2
1.4
1.6
×10⁻²
x B.D. / Re

Fig. 14.

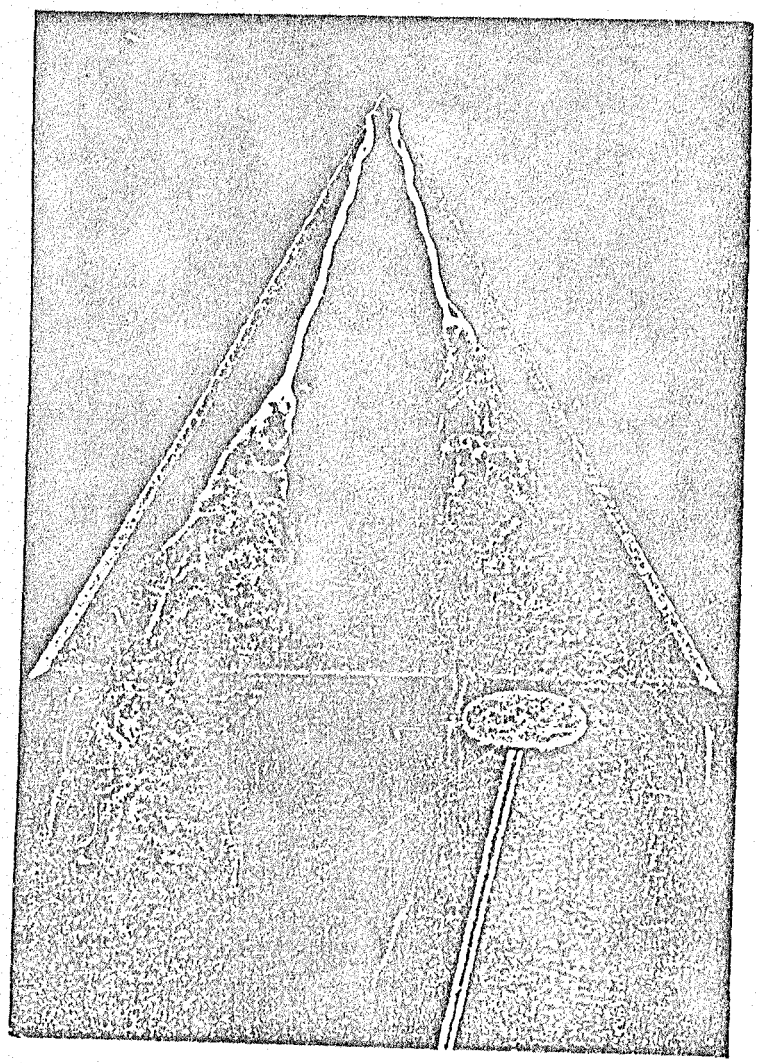

Fig. 15.

3.2. Comparison to experimental results

Faler and Leibovich [8] performed several experiments on vortices in divergent tubes. The swirl component was generated by swirl vanes and afterwards the flow was led through the tube. Profiles for the axial and circumferential velocities were measured $^1/_3$ diameter upstream of the divergent part of the tube. The opening angle for the tube was 1.43° and various mass fluxes and swirl vane angles of attack investigated. They found six different breakdown types for the flow, the corresponding breakdown lengths and their dependence on the Reynolds number and swirl parameter are shown in fig. 16. The Reynolds number is based here on the averaged axial velocity and the diameter of the tube.

Since the slender vortex approximation only deals with axisymmetric flows, only bubble-type breakdown is considered in this comparison (types "0" and "1" according to the terminology used in [8]). Stable bubble structures are only present for certain ranges of circulation ω and Reynolds number Re.

One more inconvenience causes from the lack of detailed information on the boundary layer structure for high Reynolds numbers. Fig. 16 shows the numerical and computational results combined. The initial distributions are constant along each solution curve and coincide with the experimental values only at nodes marked (*). For $\omega = 1.07$ we can see a good agreement, the trend of decreasing breakdown length for increasing Reynolds numbers is present and the numerical values are similar. For Re around 2500 and below no breakdown occur in the numerical experiments.

For $\omega = 1.54$ the numerical prediction of the breadown length decreases for increasing Reynolds number larger than 3000. This behaviour reverses itself for $1000 \leq Re \leq 3000$. For $Re < 1000$ there is no breakdown present in the numerical experiments. The prediction of the breakdown length is now far off from its experimental counterpart. The physical reason behind this phenomenon is the sensitive behaviour of the flow on pressure variations. The pressure prediction obtained from the slender vortex approximation does not take into account the influence of the bubble presence on the pressure field acting on the vortex core. We propose that a good prediction of the breakdown location can be obtained from an inviscid calculation for the vortex core with an external pressure gradient obtained from the numerical solution of the full Navier-Stokes equations without the

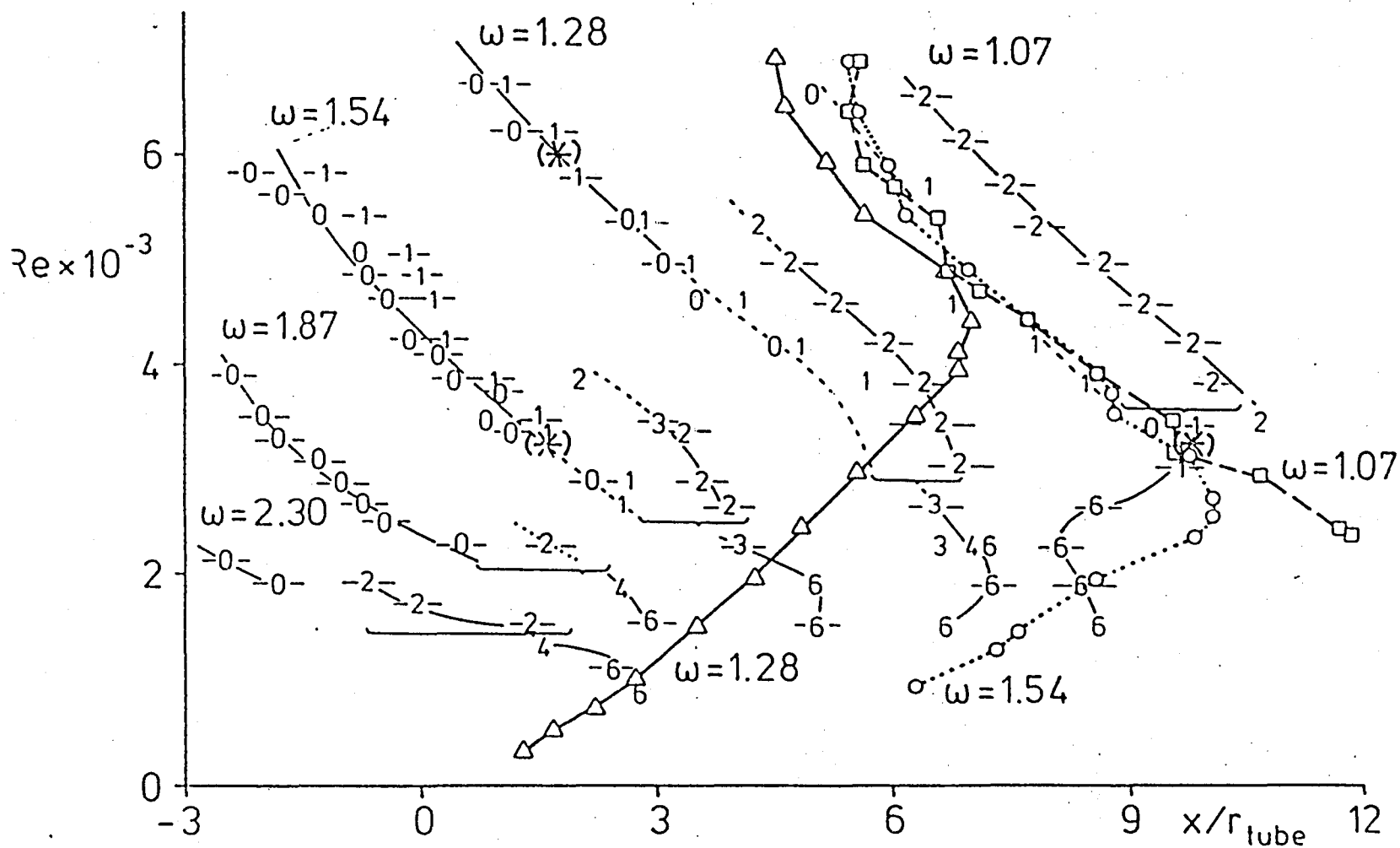
ω = 1.28
ω = 1.07
ω = 1.54
ω = 1.87
ω = 2.30
ω = 1.07
ω = 1.28
ω = 1.54
Re × 10⁻³
x/r_tube
0
2
4
6
-3
0
3
6
9
12

Fig. 16

slenderness approximation. This is an explanation for the fact that the numerical prediction strongly deviates from the experimental results. Moreover, the assumption of selfsimilar inflow profiles is not fulfilled in this case (Re = 6000). To compare with experimental data we had to assume selfsimilarity to transfer to other Reynolds numbers because only a few inflow profiles are given in [8].

The lack of upsteam influence in the approximation leads to predictions for the breakdown length which are longer than the observed values. Nevertheless, for all calculations of ω and Re the inflow profiles are supercritical and approach critical state near breakdown.

Faler and Leibovich make the following remark:
"All flows that exhibit vortex breakdown of the "axisymmetric" form (which we classify as types 0 and 1 disturbance forms) or "spiral" form (our type 2) are supercritical upstream, in the sense of Benjamin" [8].

4. Conclusions

The slender vortex approximation was studied in particular for high Reynolds numbers. For free vortices without external pressure influences the breakdown length is proportional to the Reynolds number. For free vortices with adverse pressure gradients, the breakdown length is inversely proportional to the value of its gradient. Flows with small pressure gradients take a long distance to breakdown.

For low Reynolds number the prediction of the simplified system agree quite well with the ones obtained from solutions of the full Navier-Stokes equations. It was found that the flow becomes quite sensitive on pressure fluctuations for high Reynolds numbers and that the failing of the slender vortex equations corresponds to the critical condition from Benjamin [12] for inviscid flows. The last comment holds since viscous forces are negligible near breakdown compared to inertia and pressure forces. The viscous forces do play a role for low pressure gradients by controlling the aging process. The predictions from the approximating system were compared to experimental results and for low swirl a good agreement was obtained. For higher swirl upstream effects on the pressure produced by the breakdown bubble deteriorates their agreement. This can not be incorperated into the slender vortex approximation.

Acknowledgement

This research was carried out in the frame of the special research program "Vortical Flows in Aerodynamics (SFB 25)." The authors are indebted to Professor E. Krause, Ph. D., who suggested a part of this investigation. They also thank Dr. D. Hänel for many helpful discussions.

References

1. D. H. Peckham and S. A. Atkinson, Preliminary results of low-speed wind tunnel tests on a Gothic wing of aspect ratio 1.0. Aero. Res. Counc. CP 508 (1957).

2. H. Chevalier, Flight test studies of the formation and dissipation of trailing vortices. J. Aircraft 10, 14-18 (1973).

3. A. J. Bilanin and S. E. Widnall, Aircraft wake dissipation by sinusoidal instability and vortex breakdown. AIAA paper 73-107 (1973).

4. J. Swithenbank and N. Chigier, Vortex mixing for supersonic combustion. Proc. 12th Symp. Combust. Inst., 1153-1162, Pittsburgh: Combust. Inst. (1969).

5. H. Ludwieg, Vortex breakdown. Dtsch. Luft Raumfahrt Rep. 70-40 (1970).

6. M. G. Hall, Vortex breakdown. Ann. Rev. Fluid Mech., Vol. 4, 195-218 (1972).

7. S. Leibovich, The structure of vortex breakdown. Ann. Rev. Fluid Mech., Vol. 10, 221-246 (1978).

8. J. H. Faler and S. Leibovich, Disrupted states of vortex flow and vortex breakdown. Phys. Fluids, Vol. 20, 1385-1400 (1977).

9. S. Leibovich and H. Y. Ma, Soliton propagation on vortex cores and the Hasimoto soliton. Phys. Fluids, Vol. 26, 3173-3179 (1983).

10. H. Ludwieg, Zur Erklärung der Instabilität der über angestellten Delta-Flügeln auftretenden freien Wirbelkerne. Z. Flugwiss. 13, 437-442 (1965).

11. H. B. Squire, Analysis of the vortex breakdown phenomenon. Part 1. Aero. Dept., Imperial Coll., London, Rep. 102 (1960). Also in Miszellaneen der Angewandten Mechanik, Berlin, Akademie Verlag, 306-312 (1960).

12. T. B. Benjamin, Theory of the vortex breakdown phenomenon. J. Fluid Mech. 14, 593-629 (1962).

13. T. B. Benjamin, Some developments in the theory of vortex breakdown. J. Fluid Mech. 28, 65-84 (1967).

14. H. H. Bossel, Inviscid and viscous models of the vortex breakdown phenomenon. Rep. AS-67-14, Ph. D. thesis, Univ. Calif., Berkeley (1967).

15. H. H. Bossel, Vortex breakdown flowfield. Phys. Fluids, Vol. 12, 498-508 (1969).

16. Z. Lavan, H. Nielsen and A. A. Fejer, Seperation and flow reserval in swirling flows in circular ducts. Phys. Fluids, Vol. 12, 1747-1757 (1969).

17. R. M. Kopecky and K. E. Torrance, Initiation and structure of axisymmetric eddies in a rotating stream. Comput. Fluids 1, 289-300 (1973).

18. W. J. Grabowski and S. A. Berger, Solutions of the Navier-Stokes equations for vortex breakdown. J. Fluid Mech. 75, 525-544 (1976).

19. J. H. Faler and S. Leibovich, An experimental map of the internal structure of a vortex breakdown. J. Fluid Mech. 86, 313-335 (1978).

20. X. G. Shi, Numerische Simulation des Aufplatzens von Wirbeln, Ph. D. thesis, RWTH Aachen, Aachen (1983).

21. I. S. Gartshore, Recent work in swirling incompressible flow. NRC Can. Aero. Rep. LR-343 (1962).

22. I. S. Gartshore, Some numerical solutions for the viscous core of an irrotational vortex. NRC Can. Aero. Rep. LR-378 (1963).

23. M. G. Hall, A numerical method for solving the equations for a vortex core. Aero. Res. Counc. R. & M. 3467 (1965).

24. M. G. Hall, The structure of concentrated vortex cores. Prog. Aeronaut. Sci., Vol. 7, 53-110 (1966).

25. M. G. Hall, A new approach to vortex breakdown. Proc. 1967 Heat Transfer Fluid Mech. Inst., Stanford Univ. Press, 319-340 (1967).

26. H. H. Bossel, Vortex computation by the method of weighted residuals using exponentials. AIAA J. 9, 2027-2034 (1971).

27. A. Mager, Dissipation and breakdown of a wing-tip vortex. J. Fluid Mech. 55, 609-628 (1972).

28. Y. Nakamura and S. Uchida, Calculations of axisymmetric swirling flows by

29. E. Krause, L. Reyna and S. Menne, Druckänderung bei axialsymmetrischem Wirbelaufplatzen. Abh. Aerodyn. Inst. RWTH Aachen 27, 1-10 (1985).

30. H. Werlé, Sur l'eclatement des tourbillons d'apex d'une aile delta aux faibles vitesses. La Rech. Aérosp. No. 74, 23-30 (1960).

31. S. Menne, Approximation für schlanke Wirbel mit diskontinuierlichen Anfangsverteilungen, paper submitted for presentation at the GAMM-Tagung, Dortmund 1986.

Fig. 1: Coordinate system and grid definition

Fig. 2: Stability diagram for vortex breakdown

—△— Transition from super- to subcritical flow according to Benjamin [12]

—□— Breakdown at inflow section for slender vortex approximation, initial condition (20)

////// Region of temporary stable vortices

---- Breakdown at inflow section for slender vortex approximation, initial condition (25)

Fig. 3: Axial variation of the inertia, pressure, and viscous forces per unit volume as computed with the viscous slender-vortex approximation

Fig. 4: Radial profiles of the axial, radial, and circumferential velocity components computed with viscous slender-vortex approximation

Fig. 5: Radial profiles of the static pressure as computed with viscous slender-vortex approximation

Fig. 6: Axial variation of the axial velocity component and of the static pressure as computed with the viscous slender-vortex approximation

Fig. 7a: Axial velocity profiles computed with slender vortex approximation for inviscid flow

Fig. 7b: Radial velocity profiles computed with slender vortex approximation for inviscid flow

Fig. 7c: Circumferential velocity profiles computed with slender vortex approxi-

Fig. 8: Pressure profiles computed with slender vortex approximation for inviscid flow

Fig. 9: Axial pressure variation computed with slender vortex approximation for inviscid flow

Fig. 10: Shape parameter α as a function of the breakdown length. Computed for several swirl rates

Fig. 11: Axial variation of the axial velocity component computed with viscous slender vortex approximation

Fig. 12a: Breakdown length as a function of the Reynolds number for constant externally imposed pressure gradient τ. Computed with viscous slender-vortex approxiamtion

Fig. 12b: Breakdown length as a function of imposed external pressure gradient τ for constant Reynolds number. Computed with viscous slender vortex approximation

Fig. 13a: Same as Fig. 12a. The swirl parameter $\beta = 0.8$

Fig. 13b: Same as Fig. 12a. The swirl parameter $\beta = 0.8944$

Fig. 14: Influence of an externally imposed axial pressure gradient τ on the breakdown length as computed with the viscous slender-vortex approximation

Fig. 15: Influence of an externally imposed axial pressure gradient on the breakdown length. (From [30])

Fig. 16: Comparison of experimental data (from [8]) and numerical results with slender vortex approximation. The type of disturbance (0-6) and its mean axial location vs. Reynolds number.

END

DATE

FILMED

NOV 12 1986

End of Document